

การประเมินสมบัติเชิงโครงสร้างและเชิงพลวัตของไฮเดรตทโทไอซัลเฟตไอออนโดยการ
จำลองพลวัตเชิงโมเลกุลสนามประจุกลศาสตร์ควอนตัม

นางสาวมนทิรา ไตรนภากุล

วิทยานิพนธ์นี้เป็นส่วนหนึ่งของการศึกษาตามหลักสูตรปริญญาวิทยาศาสตรมหาบัณฑิต
สาขาวิชาเคมี ภาควิชาเคมี
คณะวิทยาศาสตร์ จุฬาลงกรณ์มหาวิทยาลัย
ปีการศึกษา 2556
ลิขสิทธิ์ของจุฬาลงกรณ์มหาวิทยาลัย

บทคัดย่อและแฟ้มข้อมูลฉบับเต็มของวิทยานิพนธ์ตั้งแต่ปีการศึกษา 2554 ที่ให้บริการในคลังปัญญาจุฬาฯ (CUIR)
เป็นแฟ้มข้อมูลของนิสิตเจ้าของวิทยานิพนธ์ที่ส่งผ่านทางบัณฑิตวิทยาลัย

The abstract and full text of theses from the academic year 2011 in Chulalongkorn University Intellectual Repository (CUIR)
are the thesis authors' files submitted through the Graduate School.

EVALUATION OF STRUCTURAL AND DYNAMICAL PROPERTIES OF
HYDRATED THIOSULFATE ION BY QUANTUM MECHANICAL CHARGE
FIELD MOLECULAR DYNAMICS SIMULATION

Miss Montira Trinapakul

A Thesis Submitted in Partial Fulfillment of the Requirements
for the Degree of Master of Science Program in Chemistry
Department of Chemistry
Faculty of Science
Chulalongkorn University
Academic Year 2013
Copyright of Chulalongkorn University

Thesis Title EVALUATION OF STRUCTURAL AND DYNAMICAL
 PROPERTIES OF HYDRATED THIOSULFATE ION BY
 QUANTUM MECHANICAL CHARGE FIELD MOLECULAR
 DYNAMICS SIMULATION
By Miss Montira Trinapakul
Field of Study Chemistry
Thesis Advisor Assistant Professor Viwat Vchirawongkwin, Dr. rer. nat.

Accepted by the Faculty of Science, Chulalongkorn University in Partial Fulfillment of the Requirements for the Master's Degree

.....Dean of the Faculty of Science
(Professor Supot Hannongbua, Dr. rer. nat.)

THESIS COMMITTEE

.....Chairman
(Assistant Professor Warinthorn Chavasiri, Ph.D.)

.....Thesis Advisor
(Assistant Professor Viwat Vchirawongkwin, Dr. rer. nat.)

.....Examiner
(Associate Professor Pornthep Sompornpisut, Ph.D.)

.....External Examiner
(Associate Professor Chinapong Kritayakornupong, Dr. rer. nat.)

มนทิตรา ไตรนภากุล : การประเมินสมบัติเชิงโครงสร้างและเชิงพลวัตของไฮเดรตเตตไทโอซัลเฟตไอออนโดยการจำลองพลวัตเชิงโมเลกุลสนามประจุกลศาสตร์ควอนตัม. (EVALUATION OF STRUCTURAL AND DYNAMICAL PROPERTIES OF HYDRATED THIOSULFATE ION BY QUANTUM MECHANICAL CHARGE FIELD MOLECULAR DYNAMICS SIMULATION) อ.ที่ปรึกษาวิทยานิพนธ์หลัก : ผศ. ดร.วิวัฒน์ วชิรวงศ์กวิน, 59 หน้า.

การจำลองพลวัตเชิงโมเลกุลสนามประจุกลศาสตร์ควอนตัม (QMCF MD) สามารถใช้ตรวจสอบสมบัติของไฮเดรตซันเซลล์เชิงโมเลกุลเพื่อศึกษาการเกิดปฏิกิริยาของไทโอซัลเฟต ($S_2O_3^{2-}$) ไอออน โครงสร้างเฉลี่ยของไอออนระบุผลกระทบอย่างมีนัยสำคัญของโมเลกุลน้ำต่อการหดสั้นลงของความยาวพันธะของ S – S ซึ่งส่งผลทำให้สเปกตรัมในโหมดการสั่นแบบยืดของพันธะนี้ ($\nu(SS)$) เกิดการแตกสัญญาณออกเป็นพีกย่อย การตรวจสอบเพิ่มเติมโดยโมเดลอย่างง่ายด้วยทฤษฎีระดับต่างๆ แสดงสมบัติไม่ชอบน้ำของพันธะ S – S การประเมินจำนวนโคออร์ดิเนชันเชิงโมเลกุลขึ้นกับรัศมีของไฮเดรตซันเชิงอะตอมซึ่งได้ค่าจากขอบเขตที่คลุมเครือของพีกแรกในฟังก์ชันการกระจายตัวของรัศมีเชิงอะตอม จำนวนการสัมผัสโดยตรงระบุน้ำจำนวน 6.8 โมเลกุลที่เกิดอันตรกิริยากับไทโอซัลเฟตไอออน และมีน้ำส่วนเกินอีก 2.4 โมเลกุลที่อยู่ภายในไฮเดรตซันเซลล์เชิงโมเลกุลซึ่งสร้างโครงข่ายพันธะไฮโดรเจนกับบัลด์ ค่าเรสซิเดนซ์ไทม์เฉลี่ยของน้ำจำแนกความแข็งแรงแบบอสมมาตรของไฮเดรตซันเซลล์เป็นด้านอะตอมซัลเฟอร์แข็งแรงน้อยกว่าและออกซิเจนทั้งสามอะตอมแข็งแรงมากกว่า ซึ่งกระตุ้นอะตอมซัลเฟอร์ตำแหน่งปลายเป็นด้านที่ว่องไวในการเกิดปฏิกิริยาเคมี

ภาควิชา.....เคมี..... ลายมือชื่อนิสิต.....
 สาขาวิชา.....เคมี..... ลายมือชื่อ อ.ที่ปรึกษาวิทยานิพนธ์หลัก.....
 ปีการศึกษา.....2556.....

5373817123 : MAJOR CHEMISTRY

KEYWORDS : THIOSULFATE / DYNAMICAL PROPERTIES / AB INITIO / QMCF / SIMULATION

MONTIRA TRINAPAKUL : EVALUATION OF STRUCTURAL AND DYNAMICAL PROPERTIES OF HYDRATED THIOSULFATE ION BY QUANTUM MECHANICAL CHARGE FIELD MOLECULAR DYNAMICS SIMULATION. ADVISOR : ASST. PROF. VIWAT VCHIRAWONGKWIN, Dr. rer. nat., 59 pp.

The reactivity of terminated sulfur atom within the thiosulfate ($S_2O_3^{2-}$) ion involving in chemical reactions was investigated by the properties of molecular hydration shell obtained from the *ab initio* quantum mechanical charge field molecular dynamics (QMCF MD) simulation. The average geometry indicated the significant effect of explicit water molecule on the reduction of S – S length, reflecting in the splitting peaks of the spectrum for the stretching mode of this bond ($\nu(SS)$). A further investigation on a simple model with various theoretical levels exhibited the hydrophobicity of the S – S bond. The evaluation of molecular coordination number was sensitive with the radius of atomic hydration spheres, obtained from vague boundaries of the first peak in the atomic radial distribution functions. The number of actual contacts specified 6.8 water molecules interacting to the thiosulfate ion, and 2.4 extra waters located in the molecular hydration shell forming H-bonds network with bulk. The mean residence times for the water ligands distinguished the asymmetric strength of hydration shell into a weaker sulfur and three stronger oxygen sites, instigating the terminated sulfur atom as the active site involving in chemical reactions.

Department :Chemistry..... Student's Signature.....

Field of Study :Chemistry..... Advisor's Signature.....

Academic Year :2013.....

ACKNOWLEDGEMENTS

This project was not successfully finished without the support and help from my advisor. I would like to express my deep gratitude to Assist. Prof. Dr. Viwat Vchirawongkwin for his valuable and constructive suggestions during this research work, encouragement to do this project, and introducing me to another world of chemistry: the computational simulation.

I would like to acknowledge Assist. Prof. Dr. Warinthorn Chavasiri, Assoc. Prof. Dr. Pornthep Sompornpisut and Assoc. Prof. Dr. Chinapong Kritayakornupong, who are the committee of this thesis.

The fully financial support provided by the Development and Promotion of Science and Technology (DPST) scholarship throughout the academic program was greatly appreciated.

This work reported in this thesis was performed at the Department of Chemistry, Faculty of Science, Chulalongkorn University, Thailand. I am grateful to study here and thankful for the support in the electricity for computer server to execute the calculations.

My special thanks are extended to the staff member (coordinator) of the Department of Chemistry, Ms. Piyawan Kilnraruay for enabling me to visit the office, and explanation and management the documents for the department and faculty.

I would also like to thank my parents and family for their encouragement.

Moreover, I also wish to thank the group members, Mr. Thitiphong Meenayothin, Mr. Chokchai Pornpiganon and Mr. Pavares Charoenchaiyikul for their continuous support, assistance and discussions during these years.

CONTENTS

	Page
ABSTRACT IN THAI	iv
ABSTRACT IN ENGLISH	v
ACKNOWLEDGEMENTS	vi
CONTENTS	vii
LIST OF TABLES	ix
LIST OF FIGURES	x
CHAPTER I INTRODUCTION	1
1.1 The Applications of Thiosulfate	1
1.2 The Investigations of Thiosulfate	2
1.2.1 The Experimental Investigations of Thiosulfate	2
1.2.2 The Theoretical Investigations of Thiosulfate	3
CHAPTER II METHODS	5
2.1 Theories	5
2.1.1 Quantum Mechanics	5
2.1.2 Molecular Mechanics	8
2.1.3 Molecular Dynamics	10
2.1.4 Quantum Mechanical Charge Field Molecular Dynamics	11
2.2 Computational Details	13
2.3 Structural and Dynamical Properties	15
2.3.1 Radial Distribution Function	15
2.3.2 Coordination Number Distribution	16
2.3.3 Angular Distribution Function	16
2.3.4 Mean Residence Time	16
2.3.5 Velocity Autocorrelation Function	17
2.3.6 Three-dimensional alignment via Contravariant Transformation	18

	Page
CHAPTER III RESULTS AND DISCUSSIONS	22
3.1 Verification of Method: Water Models and Basis Sets	22
3.2 Structural and Dynamical Properties of Thiosulfate Ion	26
3.2.1 Structural Parameters and Geometry	27
3.2.2 Vibrational Spectra	31
3.3 Structural and Dynamical Properties of the Hydration Shell	35
3.3.1 The Atomic Hydration Shell	35
3.3.2 The Molecular Hydration Shell	38
3.3.3 Actual Coordination Number	41
3.3.4 Mean Residence Time (MRT)	43
3.3.5 Dynamics of the Water Molecules	46
CHAPTER IV CONCLUSION	48
REFERENCES	57
VITAE	58

LIST OF TABLES

Table		Page
3.1	Vibrational frequencies of water molecules in the QM and MM (bulk) regions. The values of QM region were scaled by the factor of 0.902 presented in parentheses.	24
3.2	Percentage error of binding energies obtained from MP2, MP4(SDQ) and CCSD calculations compared with the value of HF level. The values in parentheses present the percentage error including the basis set superposition error (BSSE) according to Boys-Bernardi procedure.	26
3.3	The structural parameters for the geometry of $S_2O_3^{2-}$ ion obtained from the average of their distributions with variations	28
3.4	The bond distances (Å) within the optimized geometries of $S_2O_3^{2-}$ ion in gas and PCM phases obtained from various theoretical levels	30
3.5	Vibration frequencies (cm^{-1}) of highest peak for each normal mode of $S_2O_3^{2-}$ ion evaluated by the VACFs of QMCF MD simulation, given as values scaled by the factor 0.902 in parentheses	35
3.6	Characteristic values of the radial distribution function $g_{\alpha\beta}(r)$ for each site of $S_2O_3^{2-}$ ion in the hydration shell determined by the QMCF MD simulation	37
3.7	Average number of hydrogen bonds for each coordinating site and molecular hydration of $S_2O_3^{2-}$ ion in the simulation period	42
3.8	Mean ligand residence time τ (ps), number of accounted ligand exchange events N and total number of processes needed for one successful water exchange R_{ex} obtained from the QMCF MD simulation	44

LIST OF FIGURES

Figure	Page
2.1 The reference coordinate defined from the new basis vectors via the facet constructed from three oxygen atoms for each trajectory configuration	19
3.1 The $O_w \cdots O_w$ distance distribution of water molecules in the bulk . .	23
3.2 The structure I, II and III are the $[S_2O_3(H_2O)_n]^{2-}$ ($n = 1, 3$ and 6) clusters obtained from the geometry optimization at the HF level and the selected configuration from the QMCF MD trajectories (structure IV), employing to evaluate the binding energy at the MP2, MP4(SDQ) and CCSD levels.	25
3.3 All superimposed trajectories for the coordinates of $S_2O_3^{2-}$ ion (a) without and (b) with 3D alignment obtained from the QMCF MD simulation. The yellow spheres are the sulfur, and red spheres are the oxygen atoms	27
3.4 The average geometry of thiosulfate ion constructed from the structural parameters of QMCF MD simulation	28
3.5 The relative S – S distances to its optimized model of 6.0 \AA calculation at the same theoretical level (Δd_{S-S}) were the function of the distances of $S(1) \cdots O_{\text{water}}$ ($d_{S(1) \cdots O_{\text{water}}}$) calculated at the HF (solid line), MP2 (dotted line), and QCISD (dashed line) levels	31
3.6 Raman and IR active harmonic normal modes of the thiosulfate ion in the C_{3v} symmetry	32
3.7 Power spectra of (a) $\nu_s(SO_3)$ (solid line) and $\nu_{as}(SO_3)$ (dashed line) modes, (b) $\nu(SS)$ (solid line) and $\delta_s(SO_3)$ (dashed line) modes, and (c) $\delta_{as}(SO_3)$ (solid line) and $\delta(SS)$ (dashed line) modes	34

- 3.8** The atomic RDF plots of (a) S(1) and S(2) atoms referring to black and red lines, and (b) O(3), O(4) and O(5) atoms presenting with black, red and blue lines; solid and dashed lines refer to the RDFs for the O and H atoms of water, respectively 36
- 3.9** (a) Molecular RDF plots of $S_2O_3^{2-}$ ion obtained from the QMCF MD simulation evaluated by means of the molecular domain; solid and dashed lines refer to the RDF for the O and H atoms of water, respectively. (b) The molecular hydration shell coordination number distribution of the ion 40
- 3.10** (a) Distances plot of the selected water molecule evaluated from S(2) (black solid line), O(3) (red solid line), O(4) (green solid line), and O(5) (blue solid line) sites as a function of time during the QMCF MD simulation period. (b) All superimposed trajectories for the coordination of the selected water with 3D alignment. The yellow and red spheres are sulfurs and oxygens of $S_2O_3^{2-}$, respectively, red and gray dots are the oxygen and hydrogens of the water. 47

CHAPTER I

INTRODUCTION

1.1 The Applications of Thiosulfate

Thiosulfate ($S_2O_3^{2-}$) compounds are one of the most commonly substances utilized in many fields. There are a large number of applications in a variety of industries. They are used as the effective and potential technology for gold and silver leaching in ore mine industries, due to forming a strong complex with the metal in the extraction process [1–4]. Binding silver atoms to present in film or paper also uses this ion in the photographic industries [5]. Numerous studies have been proposed the redox reaction in many kinds of works; for instance, electrochemical reaction about metal deposition on electrode via the oxidation of thiosulfate [6, 7], silver electrocrystallisation [8, 9] and synthesis of silver nanoparticles. The shape transformation from triangular nanoprisms to hexagonal nanoplates occurred after adding some sodium thiosulfate [10]. This ion also contributes in various biological processes [11–13]. Especially in agriculture, thiosulfate (TS) liquid fertilizers provide a source of sulfur (S) and also contain other nutrients in many forms of thiosulfate; for example, nitrogen as ammonium thiosulfate (ATS), potassium as potassium thiosulfate (KT-S), calcium as calcium thiosulfate (CaTS) and magnesium as magnesium thiosulfate (MgTS). When mixing ATS with urea ammonium-nitrate (UAN), it can inhibit and decrease the rate of urea hydrolysis, which is the conversion of urea to ammonium (NH_4^+), and reduce the loss of ammonia (NH_3) as a gas after application to soil by the formation and presence of the intermediate tetrathionate ($S_4O_6^{2-}$) as the urease inhibitor not by thiosulfate itself [14, 15]. Moreover, thiosulfate ion also influences on the inhibition of nitrification, which is the conversion of NH_4^+ to nitrate, in the presence of ATS. [15] Atmospheric emission of the soil fumigant methyl bromide (CH_3Br) causes the stratospheric ozone depletion and toxicological effects on hu-

mans [16], and 1,3-dichloropropene (1,3-D) has toxicity and carcinogenicity [17]. ATS has a potential surface amendment to reduce CH_3Br volatilization from soil fumigation [16] and can transform 1,3-dichloropropene (1,3-D) in soil to non-volatile ions, which are less toxic [17].

1.2 The Investigations of Thiosulfate

1.2.1 The Experimental Investigations of Thiosulfate

The spectroscopic investigations by both IR and Raman of thiosulfate compounds have been studied by many experiments [18–20]. Church and Evans [21] observed the reaction of sodium tetrathionate with cysteine at pH 5 at the boil and room temperature by the Raman and infrared spectra investigation. They also studied the referenced compounds, *e.g.* sodium thiosulfate pentahydrate in solid state and the others to compare the spectra with the results from the reaction and the literature. Rintoul *et al.* analyzed the surface-enhanced Raman scattering (SERS) for a series of inorganic sulfur oxoanions on a dry silver-surfaced electrode by means of their own developed technique for preparing the silver surface [22]. They interested in the SERS applications and the simple structures of the anions, resulting to simple Raman spectra that can be interpreted easily. The surface-enhanced Raman data indicated the interaction between the terminated sulfur atom of thiosulfate and silver ion [22]. Raman studies of the catalyst on the electron transfer reaction between hexacyanoferrate(III) and thiosulfate ions with platinum nanoparticles clarified the binding between the platinum nanoparticle surface and the sulfur atom of thiosulfate ion [23]. The extended X-ray absorption fine structure (EXAFS) investigation on gold(I) thiosulfate complex, $\text{Au}(\text{S}_2\text{O}_3)_2^{3-}$, reported that gold was coordinated by two sulfurs [24]. Furthermore, the solutions of $\text{Cu} - \text{S}_2\text{O}_3 - \text{Cl}$ systems investigated by the EXAFS showed the coordinating of Cu(I) to sulfur atoms [25]. From these experimental results, they can be noticed that the part of the thiosulfate ion interacting with metal ions in chemical reactions is the terminated sulfur. Although thiosulfate molecule has the other three oxygen atoms, there is no reaction here.

1.2.2 The Theoretical Investigations of Thiosulfate

The first theoretical investigation was performed on the gaseous thiosulfate ion. The studies at MP2, MP4 and B3LYP with 6-31+G* levels suggested the terminated sulfur to be a stronger nucleophile as well as a stronger base than the oxygen atoms [26]. However, the highly correlated method at QCI level predicted the negative value of second electron affinity for the thiosulfate ion, suggesting that the ion is unstable in the gas phase [27,28]. As thiosulfate compounds are highly soluble in water indicating the stability in the aqueous solution, the reaction of thiosulfate ion also occurs in the solution phase where the abundance of water molecules within an aqueous solution affects on the chemical reactions. Although the thiosulfate is commonly used in aqueous solutions in many fields, there are a few experimental and theoretical studies of this ion. Therefore, the main aims of this work are to study the behavior and the interaction between thiosulfate and water, and also the vibration of thiosulfate solvated by water molecules by means of the computational calculation technique leading to be able to explain the structural and dynamical properties of hydrated thiosulfate anion.

The molecular dynamics (MD) simulation is one effective tool to acquire the properties of hydrated ion; thus, the *ab initio* quantum mechanical charge field molecular dynamics (QMCF MD) formalism [29,30] was utilized to simulate the aqueous thiosulfate system. The method includes *N*-body effects, describing the interaction between the ion and surrounding water molecules to obtain the hydration structure in the equilibrium state. About the hydration properties of this ion, there is only an experiment by the measurement of ultrasonic velocities as the functions of concentration and temperature to estimate the hydration number of aqueous sodium thiosulfate [31]. Furthermore, the results of QMCF MD simulation provide the average geometry of the hydrated thiosulfate ion; unfortunately, the experimental data of structural parameters for this ion in the solution phase are unavailable. However, there are many available data of crystal structures determined by X-ray and neutron diffraction technique from various thiosulfate salts [32–42]. The vibrational spectra from the normal modes of the thiosulfate ion were calculated and compared with the experimental results in Raman and IR spectra obtained from the sodium

or ammonium thiosulfate in aqueous solutions [19,20,22,43]. Here, the hydration structures and dynamics were evaluated to investigate the role of water molecules within the hydration shell on the specification of the active site in thiosulfate ion. Finally, the active site of thiosulfate in chemical reactions is at the terminated sulfur atom.

CHAPTER II

METHODS

Since the computers are now widespread used in many branches of science, there is a new field called "computational chemistry", using the computer as an experimental tool and employing the quantum chemistry as the method to calculate. The computational chemistry focuses on obtaining results relevant to chemical problems, not directly at developing new theoretical methods. The quantum chemistry is useful for the systems hard to study by experiment. There are a large number of theoretical levels to be applied for predicting the systems giving the results in agreement with the experimental data with accuracy and precision varying with consumable time. One of the main problems in the computational chemistry is the selection of a suitable level of theory for a given problem, and to be able to evaluate the quality of the obtained results.

2.1 Theories

2.1.1 Quantum Mechanics

Quantum mechanics (QM) is the mathematical description for the behavior of electrons, predicting the observable chemical properties from first principles. It is the basis for nearly all computational chemistry methods. In theory, QM can predict any property of an individual atom or molecule exactly. However, the QM equations have only been solved exactly for one electron systems. The well-known formulation of QM was devised by Erwin Schrödinger called "Schrödinger equation":

$$\hat{H}\Psi = E\Psi, \tag{2.1}$$

where \hat{H} is the Hamiltonian operator, Ψ is a wave function depending on the electron and nuclear positions, and E is the total energy. In the mathematics, this equation form is called an eigen value equation. Ψ is the eigenfunction, and E is an eigenvalue of the Hamiltonian operator. The operator and eigenfunction might be a matrix and vector, respectively.

The microscopic systems are described by the "wave functions" that completely characterize all of the physical properties of the system. Particularly, quantum mechanical "operators" correspond to each physical observation that allow the wave function when applied it to predict the probability of system to exhibit a particular value or range of values (scalar, vector, *etc.*) for that observation.

The Hamiltonian operator (\hat{H}) is

$$\hat{H} = - \sum_i^{\text{particles}} \frac{\nabla_i^2}{2m_i} + \sum_{i<j}^{\text{particles}} \sum \frac{q_i q_j}{r_{ij}}, \quad (2.2)$$

$$\nabla_i^2 = \frac{\partial^2}{\partial x_i^2} + \frac{\partial^2}{\partial y_i^2} + \frac{\partial^2}{\partial z_i^2}, \quad (2.3)$$

where ∇_i^2 is the Laplacian operator acting on the particle i (particles are both electrons and nuclei). The symbols m_i and q_i are the mass and charge of particle i , and r_{ij} is the distance between particles. The first term in equation (2.2) gives the kinetic energy of the particle within a wave formulation. The second term is the energy due to Coulombic attraction or repulsion of particles. This formulation is the time-independent, nonrelativistic Schrödinger equation. Additional terms can appear in the Hamiltonian when relativity or interactions with electromagnetic radiation or fields are taken into account. Unfortunately, the Schrödinger equation can be solved analytically only for a few simple one-electron systems (a hydrogen-like atom) such as the one-electron hydrogen atom. The many-electron systems (other more electron systems) must be solved by introducing the approximations.

Recently, the Hamiltonian above is nearly never used. An approximation is used to realize that the motion of the nuclei is slow compared to the motion of the electrons due to the large difference in mass. The problem can be simplified by separating the nuclear and electron motions, because the electrons are very light

particles and cannot be described by classical mechanics. On the other hand, the nuclei are sufficiently heavy displaying only small quantum effects. The large mass difference indicates that the nuclear velocities are much smaller than the electron velocities, and the electrons, therefore, adjust very fast to a change in the nuclear geometry. For a general N -particle system, the Hamiltonian operator contains kinetic (\hat{T}) and potential (\hat{V}) operators for all particles.

$$\hat{H} = \hat{T} + \hat{V} \quad (2.4)$$

$$\hat{T} = \sum_{i=1}^N \hat{T}_i = - \sum_{i=1}^N \frac{1}{2m_i} \nabla_i^2 \quad (2.5)$$

$$\hat{V} = \sum_{i>j}^N \hat{V}_{ij} \quad (2.6)$$

The approximation corresponds to neglect the coupling between the nuclear and electronic velocities, *i.e.* the nuclei are stationary from the electronic point of view. The electronic wave function; thus, depends parametrically on the nuclear coordinates, since it only depends on the position of the nuclei, not on their momentum. To a good approximation, the electronic wave function provides a potential energy surface upon which the nuclei move, and this separation is known as the *Born–Oppenheimer approximation*. The Hamiltonian for a molecule with stationary nuclei is

$$\hat{H} = - \sum_i^N \frac{\nabla_i^2}{2} - \sum_I^{nuclei} \sum_j^N \frac{Z_I}{r_{Ij}} + \sum_{i<j}^N \sum \frac{1}{r_{ij}} + \sum_{I>J}^{nuclei} \sum_J^{nuclei} \frac{Z_I Z_J}{R_{IJ}}, \quad (2.7)$$

where N is a number of the electrons. The first term is the summation of the kinetic energy for each electron. The second term is the summation of the Coulombic attraction between each electron and each nucleus. The third term is the summation of the Coulombic repulsion between all electrons. And, the summation of the repulsion between nuclei is added onto the energy at the end of the calculation in the last term. The motion of nuclei can be described by considering this entire formulation to be a potential energy surface on which nuclei move.

Due to the Born–Oppenheimer (BO) approximation, the inter-nuclear distances

are constant, therefore, the Hamiltonian of the system is reduced to become only the electronic Hamiltonian (\hat{H}^{el}) as the following equation.

$$\hat{H}^{el} = -\sum_i^N \frac{\nabla_i^2}{2} - \sum_I^{nuclei} \sum_j^N \frac{Z_I}{r_{Ij}} + \sum_{i<j}^N \sum \frac{1}{r_{ij}} \quad (2.8)$$

$$\hat{H}^{el}\psi^{el} = E^{el}\psi^{el} \quad (2.9)$$

The energy of the system is obtained by adding the inter-nuclear repulsion potential to the electronic energy.

$$E = E^{el} + \sum_{I>J}^{nuclei} \sum_J^{nuclei} \frac{Z_I Z_J}{R_{IJ}} \quad (2.10)$$

The energy is the expectation value, denoted with angled brackets $\langle \rangle$, of the Hamiltonian operator given by

$$\langle E \rangle = \int \Psi^* \hat{H} \Psi. \quad (2.11)$$

In theoretical and computational chemistry, a basis set is a set of functions (called basis functions) representing the electronic distribution function of an atom. The basis sets describe the atomic orbitals (AOs), and the linear combinations (generally as part of a quantum chemical calculation) of the basis functions create the molecular orbitals (MOs). This method is called Linear Combination of Atomic Orbitals to yield Molecular Orbitals (LCAO-MO) bonding theory to explain how atoms bond to form molecules.

2.1.2 Molecular Mechanics

The molecular mechanics (MM) energy expression consists of a simple algebraic equation for the energy of a compound. It does not use a wave function or total electron density. The constants in this equation are obtained either from spectroscopic data or *ab initio* calculations. A set of equations with their associated constants

is called a force field. The fundamental assumption of the MM methods is the transferability of parameters. In other words, the energy penalty associated with a particular molecular motion. This gives a very simple calculation that can be applied to very large molecular systems.

The energy expression consists of the sum of simple classical equations. These equations describe various aspects of the molecule, such as bond stretching, bond bending, torsions, electrostatic interactions, van der Waals forces, and hydrogen bonding. Force fields differ in the number of terms in the energy expression, the complexity of those terms, and the way in which the constants were obtained. Since electrons are not explicitly included, electronic processes cannot be modeled.

The energies computed by molecular mechanics are usually conformational energies. This computed energy is meant to be an energy that will reliably predict the difference in energy from one conformation to the next. The effect of strained bond lengths or angles is also included in this energy. This is not the same as the total energies obtained from *ab initio* methods or the heat of formation from semiempirical methods. The actual value of the conformational energy does not necessarily have any physical meaning and is not comparable between different force fields. The MM methods can be modified to compute heats of formation by including a database or computation scheme to yield bond energies that might be added to the conformational energy and account for the zero of energy.

The MM methods are not generally applicable to the structures very far from the equilibrium, such as transition structures. The algebraic expressions used in the calculations to describe the reaction path and transition structure are usually semiclassical algorithms. These calculations use an energy expression fitted to an *ab initio* potential energy surface for that exact reaction, rather than using the same parameters for every molecule.

2.1.3 Molecular Dynamics

Molecular dynamics (MD) is the time-dependent study of a molecular system, such as vibrational motion or Brownian motion. It requires a way to compute the energy of the system, most often using an MM calculation. This energy expression is used to compute the forces on the atoms for any given geometry.

Periodic Boundary Conditions

The computer simulation can predict and study the properties of a system in bulk. The system size would have to be extremely large to ensure that the surface has only a small influence on the bulk properties, but this system would be too large to simulate. The size of the system is limited by the available storage on the host computer and by the speed of execution of the program. Therefore, computer simulations are usually performed on a system with small number of molecules, $10 \leq N \leq 100$. Moreover, the bulk system usually requires the lattice to be infinite in all dimensions to avoid problems with boundary or surface effects caused by finite size. But, it is impossible to simulate a truly infinite lattice on a computer. Therefore, we have to prescribe some boundary conditions.

There are three kinds of boundaries which are periodic, reflective, and fixed value boundaries. The periodic boundary conditions (PBC) [44] are often used in computer MD simulations to simulate a part of a bulk system with no surfaces presented by modelling a small part that is far from its edge in order to eliminate the surface effects, because the molecules near the edge is similar near the surface. In PBC, a unit cell or simulation box of a geometry suitable for perfect three-dimensional tiling is defined. Periodic boundaries are obtained by periodically extending the lattice. The cubical simulation box is replicated throughout space to form an infinite lattice. In the course of the simulation, when a molecule moves in the central box, its periodic image in every one of the other boxes moves with exactly the same orientation in exactly the same way. Thus, a molecule leaves the central box, one of its images will enter through the opposite face. There are no walls at the boundary

of the central box, and the system has no surface. The central box simply forms a convenient coordinate system for measuring the locations of the N molecules. As a particle moves through a boundary, all its corresponding images move across their corresponding boundaries. Therefore, the number of particles in the central box (and hence in the entire system) is conserved. It is not necessary to store the coordinates of all images in a simulation (this would be an infinite number), just those of the molecules in the central box. When a molecule leaves the box by crossing a boundary, attention may be switched to the identical molecule just entering from the opposite side.

2.1.4 Quantum Mechanical Charge Field Molecular Dynamics

The *ab initio* quantum mechanical charge field (QMCF) molecular dynamics (MD) method is one of the formalism to study the interactions among the molecules in the interested system [29,30].

Likewise the quantum mechanical/molecular mechanical molecular dynamics (QM/MM MD) formalism, the system is separated into 2 regions: QM and MM regions. The QMCF MD has more improvement and accuracy by dividing QM region into 2 subregions: core zone and layer zone. There are both solute and some molecules of water in the core zone, while there are only solvent (water) molecules in the layer zone. And there are only solvent molecules as bulk solution in the MM region. The addition of layer zone is to neglect the non-coulombic interactions between the solute in the QM core region and solvent molecules in the MM region, because of long distance until the non-coulombic does not exist. However, there still are the non-coulombic interactions between solute and solvent molecules in the QM region [45–48]. The next advantage of QMCF is the charge field to treat the simulation as a real system from idealizing that solute is under the field of charges of the surrounding molecules. This condition, therefore, causes charge-charge interaction or also called Coulombic interaction. In order to calculate the Coulombic interactions, all atoms of the solute and solvents are set as the point charges in the system with the partial charges, for instance, one water molecule has three point charges

of one oxygen and two hydrogen atoms. However, the calculation in QM and MM region are different. In MM region, the partial charges on the atoms are fixed along the whole process of simulation. Despite the QM region, the partial charges are determined by means of the quantum calculation called "Mulliken" to evaluate new charges, resulting in changing charges of QM particles (q_i^{QM}) all the time. The fluctuation of the charges shows the dynamics of the molecules. The Coulombic force of each atom j in the MM region calculates via

$$F_j^{QM \rightarrow MM} = \sum_{i=1}^n \frac{q_i^{QM} \cdot q_j^{MM}}{r_{ij}^2}. \quad (2.12)$$

From Born-Oppenheimer (BO) approximation, all particles, that are heavy atom in comparison with electron, are included in the core Hamiltonian. Therefore, another advantage of the QMCF method is the addition of the point charges of the atoms in MM region into the core Hamiltonian via a perturbation term (V'_i):

$$V'_i = \sum_{j=1}^m \frac{q_j}{r_{ij}} \quad \text{for each particle,} \quad (2.13)$$

$$V' = \sum_{i=1}^n \sum_{j=1}^m \frac{q_j^{MM}}{r_{ij}} \quad \text{for the summation of all particles,} \quad (2.14)$$

where n is the number of atoms in the QM region, m is the number of atoms in the MM region, r_{ij} refers to the distance between a pair of particles in the QM (i) and MM (j) regions, and q_j^{MM} is the partial charges of these atoms. The values of -0.65996 and $+0.32983$ were adopted for oxygen and hydrogen charge respectively, according to the BJH-CF2 model selected for the water in the MM region.

As the conventional QM/MM MD formalism, the QMCF MD method allows the migration of water molecules between the QM and MM region using the different level of calculation. Therefore, it needs to be applied a smoothing function, $S(r)$ [49], to the atoms of all molecules located in this smoothing region by the

following conditions

$$S(r) = \begin{cases} 1 & \text{for } r \leq r_{on} & \text{(QM region),} \\ \frac{(r_{off}^2 - r^2)^2 (r_{off}^2 + 2r^2 - 3r_{on}^2)}{(r_{off}^2 - r_{on}^2)^3} & \text{for } r_{on} < r \leq r_{off} & \text{(smoothing region),} \\ 0 & \text{for } r > r_{off} & \text{(MM region),} \end{cases} \quad (2.15)$$

where r is the distance of a given solvent molecule from the centre of the simulation box, r_{off} is the radius of the QM region and r_{on} is the inner border of the smoothing region.

This function is applied to ensure that the forces of these molecules are able to change smoothly and continuously according to

$$F_j^{smooth} = F_j^{MM} + (F_j^{layer} - F_j^{MM}) \times S(r), \quad (2.16)$$

where F_j^{layer} is the force from a particle j located in the outer QM (MM region) acting on a particle in the layer zone and F_j^{MM} is the force from a particle j acting on a particle in the MM region. In this context, it has to be mentioned that energy is not rigorously conserved, but the related error can be considered minor due to the short simulation time and the large size of the quantum mechanical region.

2.2 Computational Details

The thiosulfate solution system model is performed by the QMCF MD simulation. As the experimental density value of pure water at 298 K (room temperature) is 0.997 g cm^{-3} , the density of the simulation box is set as same as the same value. This system consists of one thiosulfate ion and 495 water molecules in a cubic box of 24.68 \AA with the periodic boundary condition. The simulation is performed in the NVT ensemble using a general predictor-corrector algorithm with a time step of 0.2 fs. The system temperature is maintained at 298.16 K by the Berendsen temperature-scaling algorithm [50] with a relaxation time of 100 fs. At the center of the simulation box, the thiosulfate locates at the center surrounded with water molecules. The QM radius is set as 6.0 \AA , which is larger than size of the thiosulfate ion about 5 \AA . The

QM subregions, the core and the layer zone, is extended from the center to 3.5 and 6.0 Å, respectively. The QM calculation is performed by means of the Hartree-Fock (HF) method with the Dunning double- ζ plus polarisation (DZP) [51,52] basis sets for hydrogen, sulfur and oxygen atoms in the QM region. The thickness of the smoothing region is chosen as 0.2 Å inside from the QM radius with the values of r_{on} and r_{off} as 5.8 and 6.0 Å, respectively, according to the radial distribution function (RDF) obtained from the equilibrated simulation.

The selected water model including an intramolecular potential applied to calculate the interactions between pairs of water in the MM region is the flexible BJH-CF2 model [53,54], with the cutoff distances of 3.0 and 5.0 Å for non-Coulombic interactions between H atoms and between O and H atoms, respectively. The partial charges for oxygen and hydrogen atoms in the water molecule of the MM region are -0.65966 and $+0.32983$ according to the BJH-CF2 model. This water model supports the fully flexible molecular geometries of water molecules transiting between the QM and MM region. The Coulombic interactions between the Mulliken charges on the atoms within the QM region and the point charges of water molecules according to the BJH-CF2 model are evaluated providing an electrostatic description by a dynamically charging field of point charges, which change according to the movements of atoms inside the QM region and water molecules in the MM region in the course of the simulation. This ensures the continuous adaptation of the Coulombic interactions to all polarisation and charge-transfer effects within solute and surrounding solvent layers. [29,30] In addition, the reaction field method combined with the shifted-force potential technique are applied to account for long-range electrostatic potentials and forces, with a spherical cutoff limit of 12.350 Å. The system is initially equilibrated by the QMCF MD method for 50,000 steps (10 ps), and a further 50,000 steps (10 ps) are collected as data sampling for analysis the structural and dynamical properties.

2.3 Structural and Dynamical Properties

Due to the large number of data collected during the simulation time, it is difficult to understand and analyze the statistical representation of the raw data. So it is the better way to represent the results in various kinds of graphical representations as the following.

2.3.1 Radial Distribution Function

The radial distribution function (RDF), $g(r)$, represents the probability distribution of finding the solvent molecules interacting around the given solute atom (site) of the solute molecule at the distance r from that site compared to the ideal gas distribution following the density, ρ , in the form of frequency curve showing the solvation of the solvent. The RDF, $g_{\alpha\beta}(r)$, can be expressed as

$$g_{\alpha\beta}(r) = \frac{N_{\alpha\beta}(r)}{\frac{4}{3}\pi\rho((r + \delta r)^3 - r^3)}. \quad (2.17)$$

Atomic and Molecular RDFs

The evaluation of atomic and molecular RDFs uses different principles. Atomic RDFs acquire from each atom/site of the molecule which is assumed that its shape is sphere. We count a number of water molecules as a function of distance from the position it placed as the center and sweep around the atom spherically. To normalize atomic RDF in the process of analysis tool program we developed, it is divided by volume of a sphere $V = \frac{4}{3}\pi r^3$, whereas molecular RDF acquires from the solute molecule which its shape is not spherical. Shape of the molecule is formed by overlapping from all single spheres of each atom. Therefore, the spherical volume is not a great function to be used as the volume of the molecule. The idea to normalize is to figure out the finest method. In this work we use the numerical method by means of dividing the whole volume of the molecule into many tiny volume pieces by generating points randomly and creating small tetrahedral volume [55] within the

molecule to fulfill all inside and calculate actual volume for the normalization.

2.3.2 Coordination Number Distribution

The coordination number distribution (CND) plot shows the variation of solvation numbers during the simulation period involving with the ligand exchange processes, and represents as the histogram. The coordination numbers within the boundary are analyzed from the molecules locating in the solvation shell which is between the minima of the peak of the atomic RDFs. The atomic CND can be calculated by using the two minimum values of the peak of its own atomic RDF, while the molecular CND uses these two peak values of all atomic RDFs of the solute.

2.3.3 Angular Distribution Function

The angular distribution function (ADF) shows the probability of distinct angles among selected particles within a specified region. The intramolecular angles both bond angles and dihedral angles of solute as well as solvent molecules, showing the variation of solute and solvent geometry during the simulation period. The angles can be evaluated by the weighted mean. The ADF is used to determine the orientation of the water molecule in the first solvation shell. For the bulk system, the ADF is evaluated for comparison of the difference in geometry resulting from the presence of the solute.

2.3.4 Mean Residence Time

The mean residence time (MRT) of water molecules in the hydration shell of a solute is evaluated by means of the "direct method" [56] which counts all migrations of incoming and outgoing ligands under the condition time. The most appropriate time span to record a ligand displacement from its original coordination sphere as an exchange process is 0.5 ps [56]. This time interval also corresponds to the average

lifetime of a hydrogen bond in the solvent [57]. The mean ligand residence, τ_{ex} , is defined as

$$\tau_{ex} = \frac{t_{sim} \cdot CN_{av}}{N_{ex}}, \quad (2.18)$$

where t_{sim} is the simulation time, CN_{av} is the average coordination number of the respective shell, and N_{ex} is the number of the registered exchange events.

The ability of the solvation shell can be quantified by the number and "sustainability" of ligand exchange processes. The number of exchange events leading to a longer-lasting change in the solvation structure, $N_{ex}^{0.5}$, divided by the number of all transitions through a shell boundary, $N_{ex}^{0.0}$, defines a "sustainability coefficient", S_{ex} as the following

$$S_{ex} = \frac{N_{ex}^{0.5}}{N_{ex}^{0.0}}, \quad (2.19)$$

which reflects the success ratio of all exchange attempts, while its inverse

$$R_{ex} = \frac{1}{S_{ex}} = \frac{N_{ex}^{0.0}}{N_{ex}^{0.5}} \quad (2.20)$$

measures how many border-crossing attempts are needed to produce one long-lasting change in the hydration structure of the solute.

2.3.5 Velocity Autocorrelation Function

The data from QM/MM and QMCF MD simulations are applied in the velocity autocorrelation function (VACF) to evaluate the dynamical properties of a fluid system related to macroscopic transport coefficients, and the association with normal-coordinate analysis and Fourier transformation yielding the vibrational spectrum [58]. The VACF is a time dependent correlation function, and represents the underlying nature of dynamical processes in a molecular system. The definition of normalized

VACF, $C(t)$, is

$$C(t) = \frac{\sum_i^{N_t} \sum_j^N v_j(t_i)v_j(t_i + t)}{N_t N \sum_i^{N_t} \sum_j^N v_j(t_i)v_j(t_i)}, \quad (2.21)$$

where N is the number of particles, N_t is the number of time origins t_i , and v_j denotes a certain velocity component of the particle j . A correlation length of 2.0 ps was used to obtain the power spectra with 4000 averaged time origins for 10 ps of the simulation time.

The frequencies of vibrational ligand motions of water molecules were evaluated from the VACFs by using normal-coordinate analysis [58]. It is interesting to define the normal modes of the vibrations of the solute to predict the vibrational spectra to compare the frequencies with available experimental data.

2.3.6 Three-dimensional alignment via Contravariant Transformation

In the simulation, all molecules in the system move causing the dynamical change of their positions throughout the time. A large number of data from all configurations collected during the simulation period contain a statistical distribution, having the limitation to interpret. The visualization of the solute in the simulation period provides more details to analyze the dynamics in the system. We track the movements of waters around the thiosulfate solute by adjusting the position of the solute as the same point as the beginning, but only water molecules move around. We set the first coordination before simulation as the reference frame (Cartesian coordinate). The basis vectors \vec{i} , \vec{j} and \vec{k} along the x -, y - and z -axes, respectively, can be written in the matrix form as the following.

$$\vec{i} = \begin{bmatrix} 1 \\ 0 \\ 0 \end{bmatrix} \quad \vec{j} = \begin{bmatrix} 0 \\ 1 \\ 0 \end{bmatrix} \quad \vec{k} = \begin{bmatrix} 0 \\ 0 \\ 1 \end{bmatrix} \quad (2.22)$$

We utilize the superimposed configurations with the three-dimensional (3D) alignment by using the contravariant transformation to represent the dynamical motions

of the solute and solvent moving along the simulation time. This method can be used for molecule having more than three atoms to construct the molecular plane. Because the Cartesian coordinates of all atoms are changed in each simulation step, we set the molecular frame as shown in Figure 2.1 to define the direction to rotate them.

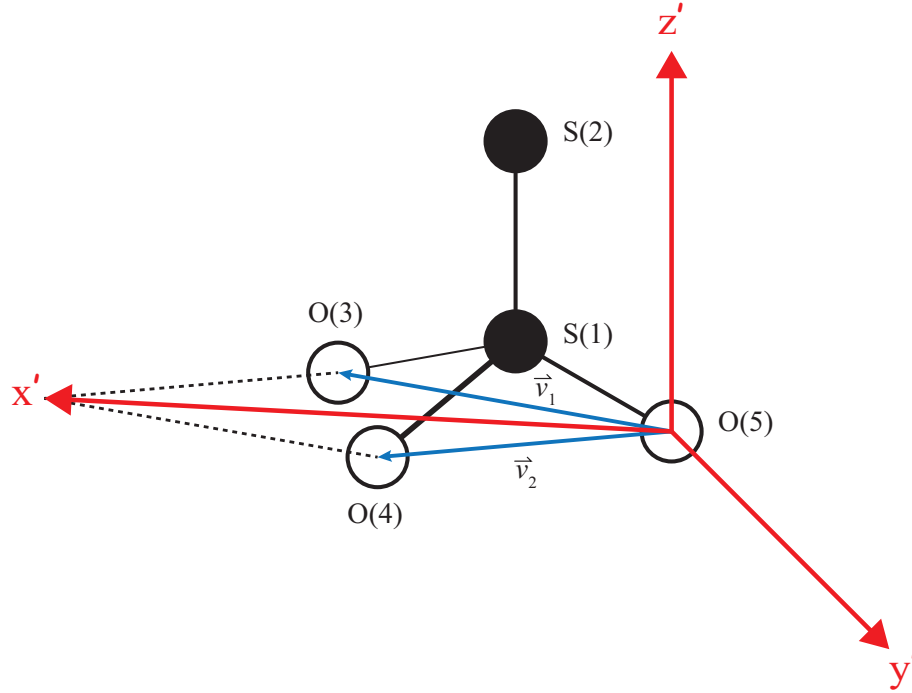


Figure 2.1: The reference coordinate defined from the new basis vectors via the facet constructed from three oxygen atoms for each trajectory configuration

The new positions of the solute in each simulation step can create the new x' -, y' - and z' -axes. We define new basis vectors via the facet constructed from three oxygen atoms for each trajectory configuration. We define \vec{v}_1 as the vector of $O(5) - O(3)$ and \vec{v}_2 as the vector of $O(5) - O(4)$. The vector \vec{v}_1 and \vec{v}_2 are on the molecular plane. We let the $S(1) - S(2)$ bond direction in the z' -axis, which is perpendicular with the plane. Therefore, the unit normal vector e_z of the facet from the cross product between the \vec{v}_1 and \vec{v}_2 defines the z' -axis, whilst the unit vector e_x from the summation of these two vectors of the vertices defines the x' -axis. Furthermore, the y' -axis is the unit normal vector e_y from the cross product of the z' - and x' -axes. The molecular frame can be represented as the following equation.

$$e_z = \frac{\vec{v}_1 \times \vec{v}_2}{\|\vec{v}_1 \times \vec{v}_2\|} \quad (2.23)$$

$$e_x = \frac{\vec{v}_1 + \vec{v}_2}{\|\vec{v}_1 + \vec{v}_2\|} \quad (2.24)$$

$$e_y = \frac{e_z \times e_x}{\|e_z \times e_x\|} \quad (2.25)$$

These vectors have three components and can be written in the matrix form as below.

$$e_x = \begin{bmatrix} e_{xx} \\ e_{xy} \\ e_{xz} \end{bmatrix} \quad e_y = \begin{bmatrix} e_{yx} \\ e_{yy} \\ e_{yz} \end{bmatrix} \quad e_z = \begin{bmatrix} e_{zx} \\ e_{zy} \\ e_{zz} \end{bmatrix} \quad (2.26)$$

These vectors have the orthogonal property. Thus, we can create the operator being the rotation matrix R that it is the unitary matrix. It can be constructed from the basis vectors e_x, e_y, e_z of the molecular frame.

$$R = \begin{bmatrix} e_x & e_y & e_z \end{bmatrix} \equiv \begin{bmatrix} e_{xx} & e_{yx} & e_{zx} \\ e_{xy} & e_{yy} & e_{zy} \\ e_{xz} & e_{yz} & e_{zz} \end{bmatrix} \quad (2.27)$$

According to the property of unitary matrix, the inverse matrix equals the transpose matrix.

$$R^{-1} = R^t \equiv \begin{bmatrix} e_{xx} & e_{yx} & e_{zx} \\ e_{xy} & e_{yy} & e_{zy} \\ e_{xz} & e_{yz} & e_{zz} \end{bmatrix} \quad (2.28)$$

The operation of the transpose of the rotation operator with each axis of the molecular frame rotate it back to the Cartesian reference axis.

$$\begin{bmatrix} e_{xx} & e_{yx} & e_{zx} \\ e_{xy} & e_{yy} & e_{zy} \\ e_{xz} & e_{yz} & e_{zz} \end{bmatrix}^t \begin{bmatrix} e_x \\ e_y \\ e_z \end{bmatrix} = \begin{bmatrix} 1 \\ 0 \\ 0 \end{bmatrix} \quad (2.29)$$

$$\begin{bmatrix} e_{xx} & e_{yx} & e_{zx} \\ e_{xy} & e_{yy} & e_{zy} \\ e_{xz} & e_{yz} & e_{zz} \end{bmatrix}^t \begin{bmatrix} e_y \\ e_z \end{bmatrix} = \begin{bmatrix} 0 \\ 1 \\ 0 \end{bmatrix} \quad (2.30)$$

$$\begin{bmatrix} \hat{R}^t \\ e_{xx} & e_{xy} & e_{xz} \\ e_{yx} & e_{yy} & e_{yz} \\ e_{zx} & e_{zy} & e_{zz} \end{bmatrix} \begin{bmatrix} e_z \\ e_{zx} \\ e_{zy} \\ e_{zz} \end{bmatrix} = \begin{bmatrix} \vec{k} \\ 0 \\ 0 \\ 1 \end{bmatrix} \quad (2.31)$$

The equation (2.29) to (2.31) proof the contravariant property of the R^t matrix.

When the rotation matrix operates on the reference vector matrix, it becomes the new vector of the new position as acquired from the simulation.

$$\hat{R}v = v' \quad (2.32)$$

On the other hand, one can rotate all atoms from the output data of the simulation by the contravariant matrix operating on the vectors of each atom in that configuration, and then become the positions which are in the same coordinate as the reference.

$$v = \hat{R}^{-1}v' = \hat{R}^t v' \quad (2.33)$$

This method can transform all points of the atoms to be as the reference that fix the atoms of the solute molecule. Therefore, the positions of the water molecules are changed in each configuration, representing the dynamics of the water molecules around the solute in the 3D figure.

CHAPTER III

RESULTS AND DISCUSSIONS

3.1 Verification of Method: Water Models and Basis Sets

According to the publication of Mark and Nilsson [59] studying the structure and dynamics of five rigid body water models: the TIP3P (original [60] and modified [61]), SPC (original [62] and refined [63]), and SPC/E (original) [64] models, they found that different water models give significantly different properties. The SHAKE algorithm [65] was applied to constrain the bond lengths including a fictitious H – H bond for making the model rigid under exactly the same condition. The results from TIP3P both original and modified models still have well-known problem, which g_{OO} of the RDF is flat and has too little structure beyond the first peak as many researches discussed before [60,61,66]. The dipole moment of the SPC/E water model is larger than the original SPC model for increasing point charges in order to give a lower potential energy, therefore, the bulk properties of the SPC/E water model are closer to the experimental values of liquid water than the original SPC model. The SPC/E water model gives the best dynamics and structure of bulk water compared with the experimental values for liquid water. Unfortunately, the interaction potentials from these five models employed in MD simulation treat the water molecules as rigid system (fixed geometry), which the parameters such as bond length and bond angle are constrained. These models are unable to simulate as the real water system, having the movement of the water *i.e.* translation, rotation and vibration.

Another well-known water model, the central force (CF) model [67] solves this problem by treating the oxygen and hydrogen atoms as dynamically distinct mass points, which have suitable electrostatic charges and subject to strictly additive pair potentials. This model uses the set of three central potentials, $V_{HH}(r)$, $V_{OH}(r)$ and $V_{OO}(r)$ to describe all atom-pair interactions in the system to determine whether the atoms belong to the same molecule. However, the vibration frequencies extremely

disagree with experiment. The modified CF models, namely CF1 [68] and CF2 [69], improve the ability to represent real water. However, they remain an error from the several mathematical restraints placed on the model. The CF2 model [69] treats the oxygen and hydrogen atoms as dynamically distinct mass points having the suitable electrostatic charges, which are subject to strictly additive pair potentials [53]. Additionally, the intra-molecular water interaction from BJH model utilizes two O–H distances and the H–O–H angle that it allows the vibration feature for the water in the MM region of previous simulations [58,70]. Therefore, the BJH–CF2 water model was selected in this research, because the combination between the BJH water model and the central force (CF2) model, namely BJH–CF2, consists of inter- and intra-molecular interaction potentials, remaining the high quality of the inter-molecular potential from the CF2 model without any modification [54].

The distance distribution for $O_w \cdots O_w$ in the bulk within the range 6–12 Å of the elementary box from the central box is evaluated and shown in Figure 3.1. The mean $O_w \cdots O_w$ distance is 2.85 Å (the center of half-height of the distribution), due to a slight asymmetry of the distribution. This distance is an excellent agreement with the experimental value of 2.88 Å [71], supporting a high quality of the BJH–CF2 water model to describe the properties of liquid water comparing with other rigid models [59].

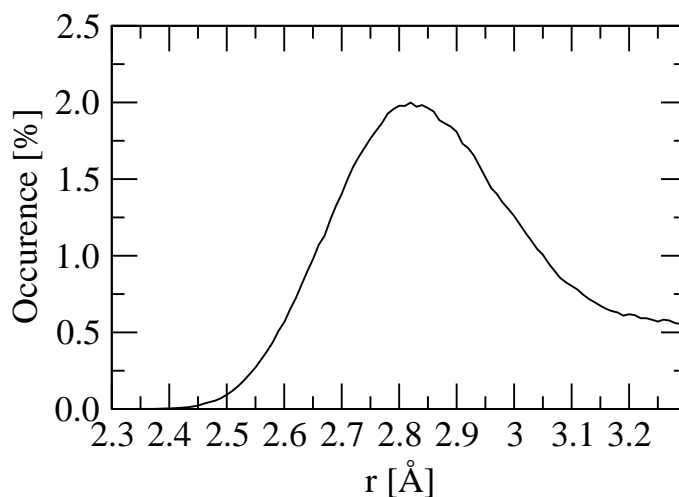


Figure 3.1: The $O_w \cdots O_w$ distance distribution of water molecules in the bulk

Table 3.1: Vibrational frequencies of water molecules in the QM and MM (bulk) regions. The values of QM region were scaled by the factor of 0.902 presented in parentheses.

	Frequency (cm^{-1})		
	Q_1	Q_2	Q_3
QM region	3811 (3438)	1792 (1616)	3844 (3467)
MM region (bulk)	3453	1694	3551
Liquid exp. [72]	3345	1645	3455

The vibrational frequencies for the normal modes of water molecules are another advantage of the BJH-CF2 model; thus, the power spectra for the symmetric (Q_1) and asymmetric (Q_3) stretching modes, and the bending mode (Q_2) of water molecules within the QM region and the bulk of the thiosulfate solution are also computed and summarized in Table 3.1. The frequencies in the bulk are consistent with those obtained in previous simulations [58,70], and are slightly higher than the experimental values for the liquid water [72]. The omission of quantum effects within the MM region attributes the differences in Q_1 and Q_3 between calculated and experimental values. The remarkable difference between the Q_3 and Q_1 frequencies of 33 cm^{-1} (29 cm^{-1} for scaled values) in the QM region compares to the values of 98 and 110 cm^{-1} from the bulk and experiment, respectively, indicating a distinct situation of water molecules within the QM region due to the interaction with the thiosulfate ion.

The decency of the selected theoretical level acquires the properties of the thiosulfate solution, verified by the comparison of percentage error in the binding energy with the correlated methods. Structure I, II and III are the testing models, each system consists of a thiosulfate ion with 1, 3 and 6 water molecules, respectively, and the structure IV is one selected configuration from the QMCF MD trajectories having 6 water molecules in the vicinity of thiosulfate ion, shown in Figure 3.2. The MP2, MP4(SDQ) and CCSD calculations are performed to evaluate the binding energy on the optimized geometries of the structure I, II and III at the HF level, and on the structure IV that it includes the effects of temperature and thermostat algorithm. Table 3.2 presents the percentage errors, obtained from MP2, MP4(SDQ)

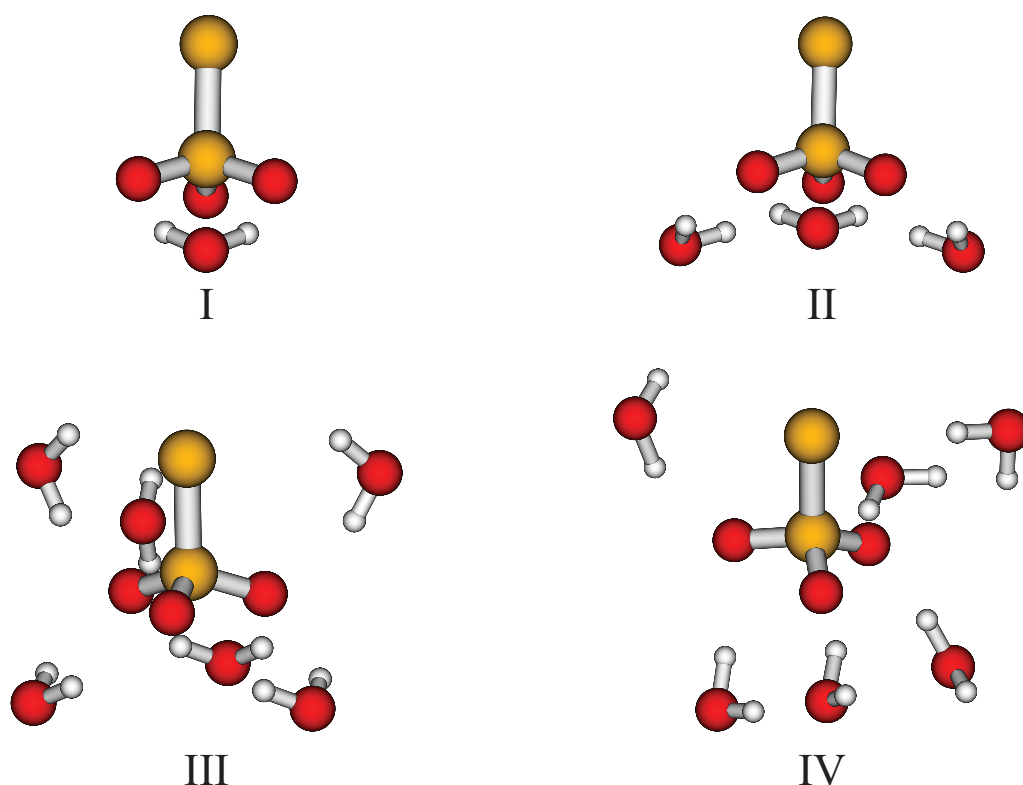


Figure 3.2: The structure I, II and III are the $[\text{S}_2\text{O}_3(\text{H}_2\text{O})_n]^{2-}$ ($n = 1, 3$ and 6) clusters obtained from the geometry optimization at the HF level and the selected configuration from the QMCF MD trajectories (structure IV), employing to evaluate the binding energy at the MP2, MP4(SDQ) and CCSD levels.

and CCSD levels which are compared with the corresponding HF energy, of binding energies and also shows with the basis set superposition error (BSSE) according to Boys-Bernardi procedure [73,74] for the testing models (Structure I, II and III) and the selected configuration (Structure IV).

As the Table 3.2, the values can be ordered from less to more as $\text{CCSD} < \text{MP4(SDQ)} < \text{MP2}$. The high correlation as MP4(SDQ) and CCSD methods supports the adequacy of the HF associating with the selected basis sets to study the aqueous thiosulfate system, according to the less percentage errors than 10% and the feasibility of recent computer. The inclusion of the effects of temperature and thermostat algorithm in the structure IV increases a percentage error by 1.1% (CCSD method) comparing with the value of structure III, suggesting a slight contribution of these effects in the simulation result. The percentage errors including the BSSE also indicate the suitability of HF level to investigate this system.

Table 3.2: Percentage error of binding energies obtained from MP2, MP4(SDQ) and CCSD calculations compared with the value of HF level. The values in parentheses present the percentage error including the basis set superposition error (BSSE) according to Boys-Bernardi procedure.

Structure	percentage error		
	MP2	MP4(SDQ)	CCSD
I	8.1 (0.2)	6.4 (1.8)	6.1 (1.7)
II	8.5 (0.1)	6.8 (1.6)	6.6 (1.4)
III	9.0 (0.6)	7.3 (1.0)	6.9 (0.9)
IV	10.9 (1.3)	8.6 (1.1)	8.0 (1.2)

3.2 Structural and Dynamical Properties of Thiosulfate Ion

The dynamical movement data of all atoms in the system were collected during the simulation. They are statistical data which are difficult to understand if demonstrate as numerical presentation. Therefore, we present the data in the easier way to comprehend as graphical representation. According to the gradient of forces, the visualization of the thiosulfate ion in the simulation period provides qualitative details of its geometric changing. In other words, the QMCF formalism allows the translation, rotation and vibration of the solute within the system. It does not have the meaning to demonstrate the superimposed configurations of this state. Thus, we eliminated the translation by selecting the sulfur atom, namely S(1), bonding with one sulfur and three oxygen atoms as the center of simulation box for each configuration, and translating all atoms by subtracting with the coordinate of the center as the 3D display in Figure 3.3a.

It shows the translated coordinates of the thiosulfate ion of all configurations. Although it illustrates the dynamics of all atoms of the thiosulfate molecule, it is unable to analyze any information from this due to the remaining of the rotation. Therefore, the three-dimensional (3D) alignment is applied by using the contravariant transformation to rotate the inner molecular reference frame constructed from the plane of three oxygen atoms of the thiosulfate ion in each configuration to the cartesian reference frame [75]. Figure 3.3b presents the superimposed configurations

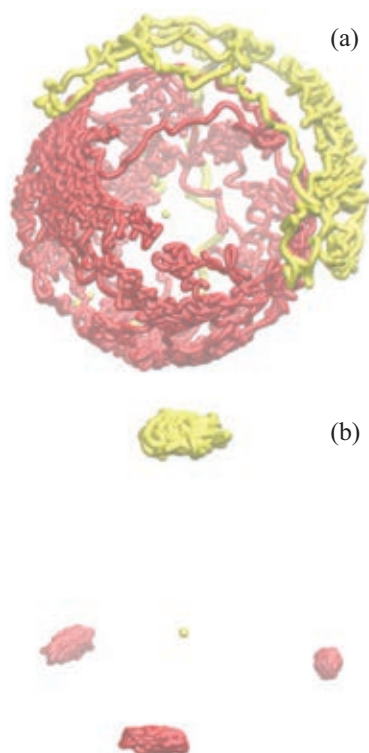


Figure **3.3**: All superimposed trajectories for the coordinates of $S_2O_3^{2-}$ ion (a) without and (b) with 3D alignment obtained from the QMCF MD simulation. The yellow spheres are the sulfur, and red spheres are the oxygen atoms

with 3D alignment. The rest of the vibration modes result in small movements for all atoms within the ion and lead to be able to predict the vibrational spectra. The coordinates of all atoms from all configurations can also be used to find the average geometry of the thiosulfate.

3.2.1 Structural Parameters and Geometry

To construct the average geometry of the thiosulfate ($S_2O_3^{2-}$) ion, it is necessary to construct the z -matrix by utilizing all structural parameters within the ion (internal solute parameters) such as bond distances, bond angles and dihedral angles from the QMCF MD result analyzed by the angular distribution functions (ADFs). The average of these parameters with statistical deviation are listed in Table **3.3** and used to construct the average geometry of the ion as shown in Figure **3.4** to compare with the experimental data.

Table 3.3: The structural parameters for the geometry of $S_2O_3^{2-}$ ion obtained from the average of their distributions with variations

Structural Parameter	QMCF MD
S(1) – S(2) (Å)	1.981 ± 0.044
S(1) – O(3) (Å)	1.487 ± 0.028
S(1) – O(4) (Å)	1.487 ± 0.030
S(1) – O(5) (Å)	1.489 ± 0.029
$\angle O(3)S(1)S(2)$ (deg)	110 ± 4
$\angle O(4)S(1)O(3)$ (deg)	110 ± 4
$\angle O(5)S(1)O(3)$ (deg)	109 ± 5
O(4)S(1)O(3)S(2) dihedral (deg)	120 ± 5
O(5)S(1)O(3)O(2) dihedral (deg)	-120 ± 5

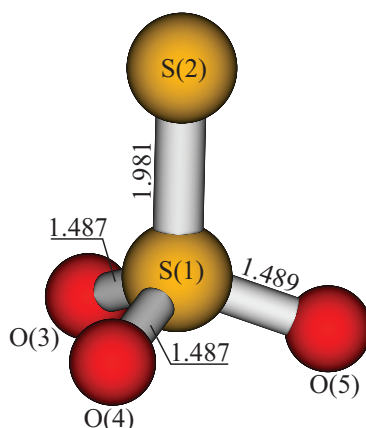


Figure 3.4: The average geometry of thiosulfate ion constructed from the structural parameters of QMCF MD simulation

The average S – S bond length is significantly longer than S – O distances due to the larger atomic size of sulfur than oxygen atom. The average values of all S(1) – O bond lengths are similar, indicating the equivalence of the oxygens and the bonds within the ion; however, there might be a slight variation in the length of S(1) – O_s bonds. All S(1) – O bond distances in the thiosulfate ion are consistent with those of sulfate (SO_4^{2-}) on the same method [76], of terminated oxygen atoms in bisulfate (HSO_4^-) [77] and in sulfonate ion (HSO_3^-) [75]. They are shorter than those (1.53 Å) within sulfite (SO_3^{2-}) obtained from QMCF MD and LAXS [78] and bisulfite (SO_3H^-) [75].

The bond and dihedral angles are collected in the form of angular distribution functions (ADFs). The bond angles around the center atom are about 110° indicating the similarity of oxygen atoms within the ion. The O – S(1) – O bond angles are approximately 110° smaller than those of bisulfate [77] which are 113° resulting from the larger sulfur than hydrogen atom.

The properties of S – S bond

The average S – S distance obtained from the QMCF result is 1.981 \AA in good agreement with many X-ray and neutron diffraction data from various thiosulfate salts in solid phase, reporting the values in the range of 1.961 to 2.024 \AA [32–42]. However, the S – S distance from the optimized geometry of this ion in the gas phase at the MP2/6-31+G(d) level is 2.093 \AA [26,27] overestimated when comparing with the X-ray and neutron diffraction data. Furthermore, according to the analysis of the hydration shell of the thiosulfate anion in Section 3.3.1, the atomic RDFs of two sulfur atoms are strange. Interestingly the RDF of the center atom S(1) is apparent showing the obvious hydration structure in spite of the fact that center atom inside the molecule surrounded with the other terminated atoms weakly interacts with water molecules unlike those ones, while the hydration structure of S(2) is unclear. Therefore, we pay attention to this circumstance. The hypothesis is the effect of water interacting with this anion. Thus, we optimize the free thiosulfate ion in both gas phase and solution phase treated with the polarizable continuum model (PCM) with various levels by using the Gaussian03 package [79] and report the bond distances in Table 3.4.

It can be noticed that all distances in the PCM are shorter than those in the gas phase, exhibiting the effect of solvent on the ion to decrease the bond distances as previous report [80]. Additionally, the average distances obtained from the QMCF MD simulation are closed to those obtained from the PCM at the same theoretical level (HF/DZP) more than any results from the gas phase. Despite the obvious effect of the explicit water molecules in the QMCF MD method on the bond length changing within the thiosulfate ion compared with the results from gas phase, this

Table 3.4: The bond distances (\AA) within the optimized geometries of $\text{S}_2\text{O}_3^{2-}$ ion in gas and PCM phases obtained from various theoretical levels

Theoretical Level	Gas		PCM	
	S – S	S – O	S – S	S – O
HF/DZP	2.049	1.482	2.011	1.480
MP2/DZP	2.068	1.525	2.015	1.523
QCISD/DZP	2.074	1.524	2.030	1.521
HF/6-31+G(d)	2.074	1.474	2.035	1.473
MP2/6-31+G(d)	2.093	1.513	2.041	1.512
QCISD/6-31+G(d)	2.096	1.511	2.054	1.509
G3MP2	2.090	1.503	2.055	1.498

method differs from the implicit solvent model of PCM approach. While the S – S bond distance from QMCF MD is shorter than from gas phase at the same theoretical level as same as the PCM, S – O bond distances are longer.

The S – O bond distances of QMCF MD slightly differ from PCM, but S – S distances are significantly different. We assume that the water might affect to the S – S more than S – O bond. The investigation, therefore, is extended into the effect of the water molecule on the S – S bond within the ion via a simple model consisting of one water molecule interacting with the S(2) atom of the thiosulfate ion in the gas phase. Using the Gaussian03 package [79], the calculations at HF, MP2 and QCISD levels with the same basis sets as the QMCF MD simulation are performed on the system. In order to fix the position of the uninterested part of the thiosulfate molecule and be able to see the dynamics of the S – S bond, we constrain $\text{S}(1) \cdots \text{O}_{\text{water}}$ distance instead of $\text{S}(2) \cdots \text{O}_{\text{water}}$ and simulate the system by varying the constrained distances of $\text{S}(1) \cdots \text{O}_{\text{water}}$ in the range of 4.5 to 6.0 \AA with a step of 0.1 \AA .

Figure 3.5 displays the change of the S – S bond length affected by the distance of the water molecule from the ion. At the beginning we set the orientation of the water molecule pointing one hydrogen atom to the ion as it should be as proven by the RDFs in section 3.3.1, whereas at the end after the optimization in the gas phase, the orientation becomes as shown in the Figure 3.5 because of the same hydrogen

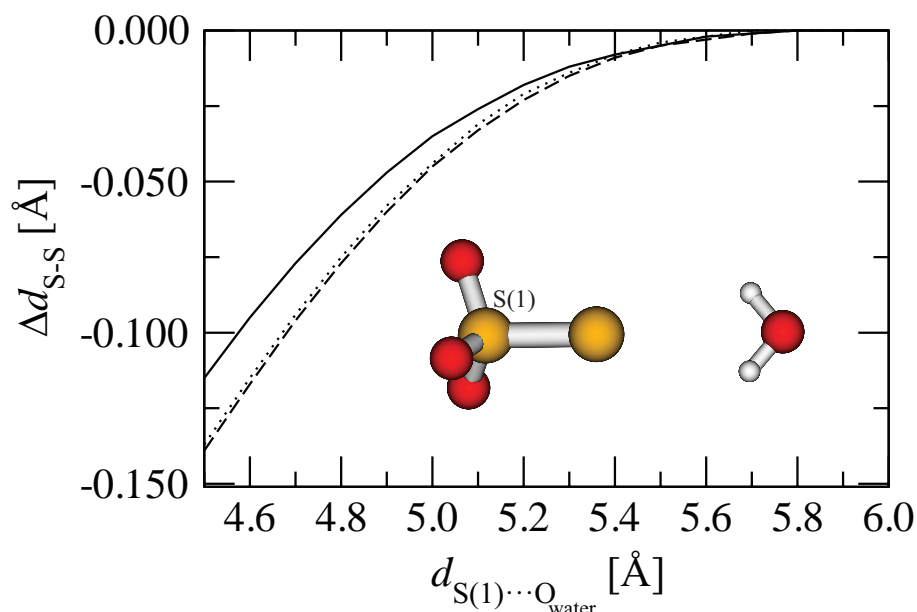


Figure 3.5: The relative S – S distances to its optimized model of 6.0 Å calculation at the same theoretical level (Δd_{S-S}) were the function of the distances of S(1) \cdots O_{water} ($d_{S(1)\cdots O_{water}}$) calculated at the HF (solid line), MP2 (dotted line), and QCISD (dashed line) levels

atoms with the same positive partial charge without any intermolecular interactions with other waters as in the QMCF MD simulation. From the graph, the more water molecule comes closer, the more S – S bond is shrunk. It presents the hydrophobic property of this bond similar to the S – H bond within the sulfonate ion [75]. This also indicates a crucial role of explicit water molecules in the solution to decrease the S – S distance.

3.2.2 Vibrational Spectra

The vibrational spectra are predicted by the VACF method. In order to obtain the vibrational frequencies corresponding to the S – S and S(1) – O vibrational motions, the velocities of all atoms of the thiosulfate ion are analyzed on the basis of Raman and IR active modes of its symmetry. As free ion, the point group of thiosulfate is C_{3v} symmetry with 6 ($3a_1 + 3e$) vibrational frequencies/bands expected from the

group theory by the following representation:

$$\Gamma_{vib}(C_{3v}) = 3a_1(\text{R, IR}) + 3e(\text{R, IR}) \quad (3.1)$$

According to the group theory, degree of freedom (DOF) for non-linear molecule is 9 from $3N-6$, where N is the number of all atoms in the molecule. In accordance with vibrational representation, $\Gamma_{vib}(C_{3v})$, a is 1 dimensional representation, and e is 2 dimensional representation, therefore, $\Gamma_{vib}(C_{3v}) = (3)(1) + (3)(2) = 9$ normal modes. However, e is doubly degenerate modes, which 2 modes overlap at the same band, resulting to 3 bands from 6 modes of e and 3 bands from 3 modes of a ; hence, the Raman and IR spectra can be predicted as only 6 bands. In order to predict the vibrational spectra by means of the QMCF MD simulation analyzing via VACFs, we assign the 6 normal modes of this solute molecule and create vectors by matching with these normal modes. All modes are Raman and IR active. The atomic motions of these modes are schematically depicted in Figure 3.6.

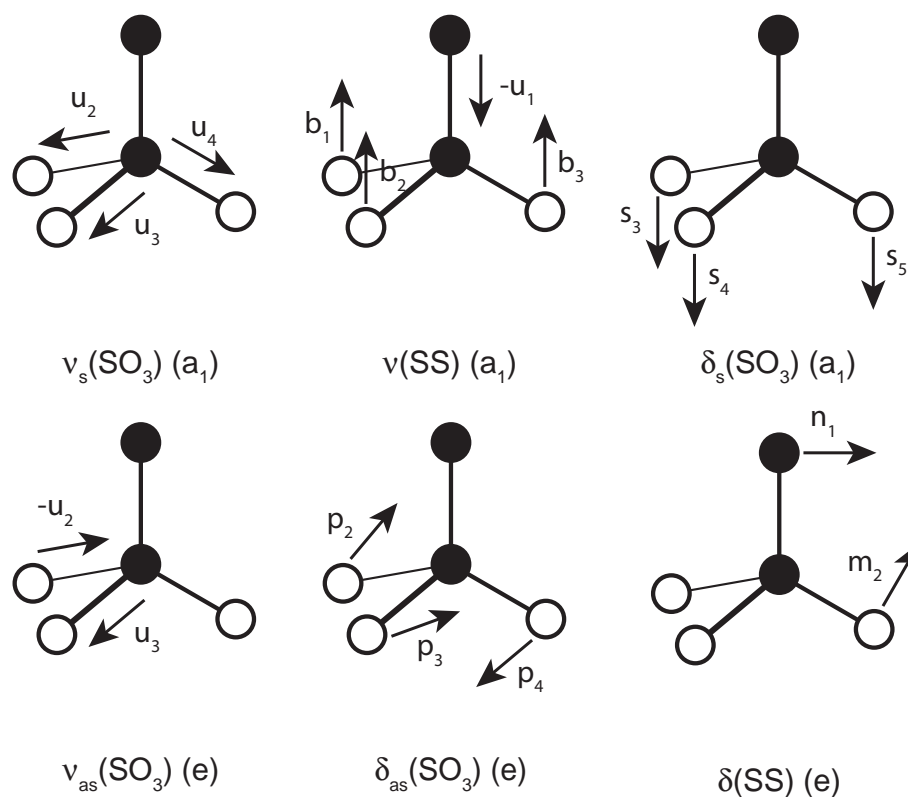


Figure 3.6: Raman and IR active harmonic normal modes of the thiosulfate ion in the C_{3v} symmetry

Although the ideal structure of the thiosulfate ion is the C_{3v} symmetry, the geometry of this molecule is changed during the simulation period. Thus, the instantaneous S and O velocities are decomposed into the necessary smallest fragments. The S(2) velocity is projected onto the unit vector parallel to the corresponding S(1) – S(2) bond (u_1) and also the O(n) velocities are projected onto the unit vector parallel to the corresponding S(1) – O(n), $n = 3 - 5$ bonds ($u_i, i = 2 - 4$) respectively.

U_i denote the projection of the S(2) or O velocity onto the unit vectors (u_i)

$$\nu_s(\text{SO}_3)(a_1) = U_2 + U_3 + U_4 \quad (3.2)$$

$$\nu(\text{SS})(a_1) = -U_1 + B_1 + B_2 + B_3 \quad (3.3)$$

$$\delta_s(\text{SO}_3)(a_1) = S_3 + S_4 + S_5 \quad (3.4)$$

$$\nu_{as}(\text{SO}_3)(e) = -U_2 + U_3 \quad (3.5)$$

$$\delta_{as}(\text{SO}_3)(e) = P_2 + P_3 + P_4 \quad (3.6)$$

$$\delta(\text{SS})(e) = N_1 + M_2 \quad (3.7)$$

The predicted spectra of the thiosulfate are displayed in Figure 3.7. Some bands show mixed modes and have more than one frequency, but the actual bands of the spectra should be isolated: one normal modes should give one frequency and each a mode should have only one frequency. These result from unclean defined vectors because of the dynamics throughout the simulation. There are mixed vibrational modes resulting from the stretching and bending of the molecules at the same time. The vectors are fluctuated with the direction change affecting to the re-orientation through the simulating time resulting in mixed mode. The highest peak and its frequency are defined to belong to that mode. The vibrational frequencies and assignments for each mode of thiosulfate are listed in Table 3.5, presenting with the scaled values in parentheses by the factor of 0.902 obtained from the correction with the coupled-cluster singles and doubles (CCSD) level [70]. The frequencies of each mode are in good agreement with the experimental data [19, 20, 22] as shown in Table 3.5, supporting that the QMCF MD simulation is a reliable tool to analyze the vibration modes of the solute to predict IR and Raman spectrum [70, 77, 81–83]. However, all calculated frequencies (without scaling) are higher than the experimental

data under 90 cm^{-1} while the scaled values are lower around 35 cm^{-1} indicating that the factor adjusts the results to be corrected values close to the spectroscopic data.

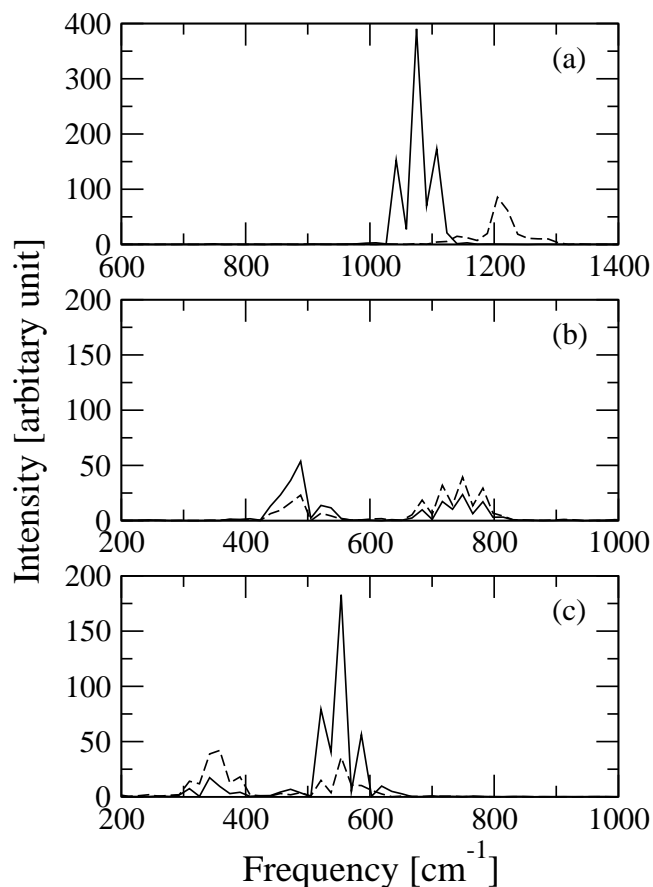


Figure 3.7: Power spectra of (a) $\nu_s(\text{SO}_3)$ (solid line) and $\nu_{as}(\text{SO}_3)$ (dashed line) modes, (b) $\nu(\text{SS})$ (solid line) and $\delta_s(\text{SO}_3)$ (dashed line) modes, and (c) $\delta_{as}(\text{SO}_3)$ (solid line) and $\delta(\text{SS})$ (dashed line) modes

Figure 3.7a shows the isolated spectra of $\nu_s(\text{SO}_3)$ and $\nu_{as}(\text{SO}_3)$ modes, corresponding to the characteristic assignment in Raman experiment [20]. The spectra in Figure 3.7b and Figure 3.7c present the mixing of the $\nu(\text{SS})$ with $\delta_s(\text{SO}_3)$ modes and the $\delta_{as}(\text{SO}_3)$ with $\delta(\text{SS})$ modes, respectively, corresponding with the normal coordinate analysis of the Raman spectra by Alvarez et al. [43] The splitting of $\nu(\text{SS})$ peak accords the susceptible changing the length of the S – S bond with the dynamics of water molecules within its hydration sphere, similar with the $\nu(\text{SH})$ spectrum of the sulfonate ion [75]. The frequency of $\delta_s(\text{SO}_3)$ is higher than the value of $\delta_{as}(\text{SO}_3)$ mode, conforming to the assignment via an accurate investigation with the isotope

Table 3.5: Vibration frequencies (cm^{-1}) of highest peak for each normal mode of $\text{S}_2\text{O}_3^{2-}$ ion evaluated by the VACFs of QMCF MD simulation, given as values scaled by the factor 0.902 in parentheses

vibration mode ^a	QMCF MD	Raman and IR
$\nu_{\text{as}}(\text{SO}_3)(e)$	1205 (1087)	1122 ^b , 1118 ^c , 1107 ^d , 1118 ^e , 1132 ^f
$\nu_{\text{s}}(\text{SO}_3)(a_1)$	1075 (970)	995 ^b , 999 ^c , 999 ^d , 995 ^e , 995 ^f
$\delta_{\text{s}}(\text{SO}_3)(a_1)$	749 (676)	663 ^b , 670 ^e , 669 ^f
$\delta_{\text{as}}(\text{SO}_3)(e)$	554 (499)	533 ^b , 538 ^e , 541 ^f
$\nu(\text{SS})(a_1)$	489 (441)	443 ^b , 448 ^c , 448 ^d , 450 ^e , 446 ^f
$\delta(\text{SS})(e)$	342 (309)	332 ^b , 337 ^c , 334 ^d , 340 ^e , 335 ^f

^aNotation of vibration modes: stretching (ν); bending (δ); symmetric (subscript s); asymmetric (subscript as).

^bRaman data of $\text{Na}_2\text{S}_2\text{O}_3$ in aqueous solution [22].

^cRaman data of 1 M $\text{Na}_2\text{S}_2\text{O}_3$ in aqueous solutions [20].

^dRaman data of 0.5 M $\text{Na}_2\text{S}_2\text{O}_3$ in aqueous solutions [20].

^eRaman data of $(\text{NH}_4)_2\text{S}_2\text{O}_3$ in aqueous solutions [20].

^fIR data of SO_3S^{2-} in the solid state [19].

effect on the IR and Raman spectra [43]. This again confirms that the combination of vector analysis with the QMCF MD result is appropriate to evaluate the power spectra of solute comparable with the experimental data.

3.3 Structural and Dynamical Properties of the Hydration Shell

3.3.1 The Atomic Hydration Shell

Radial Distribution Functions (RDFs)

The interactions of water molecules with the coordinating sites (atoms) of thiosulfate anion contribute the hydration shell covering around this solute. To study the properties of the hydration shell, the primary data of the hydration structures for each site from the QMCF MD simulation we first evaluate are the atomic radial distribution functions (atomic RDFs) as shown in Figure 3.8, representing the existence of the hydration shells of these sites. The positions of the first peak (r_{max}) and its boundary (r_{min}), in other words, the distances of the maximum and minimum probability, $g_{\alpha\beta}(r)$, of water molecules constructing hydration shell, re-

spectively, for $(\text{site}) \cdots \text{O}_{\text{water}}$ and $(\text{site}) \cdots \text{H}_{\text{water}}$ RDFs of the thiosulfate ion are listed in Table 3.6. Overall, the distances of both maximum and minimum for each $(\text{site}) \cdots \text{H}_{\text{water}}$ are obviously shorter than $(\text{site}) \cdots \text{O}_{\text{water}}$ indicating that the orientation of water molecules within the hydration shells points H_{water} atom to the coordinating sites via hydrogen bonding. The distances for $\text{S}_{\text{S}} \cdots \text{water}$ are longer than those of $\text{O}_{\text{S}} \cdots \text{water}$ showing that oxygen atom of thiosulfate (O_{S}) can attract water molecule to interact closer than sulfur atom (S_{S}).

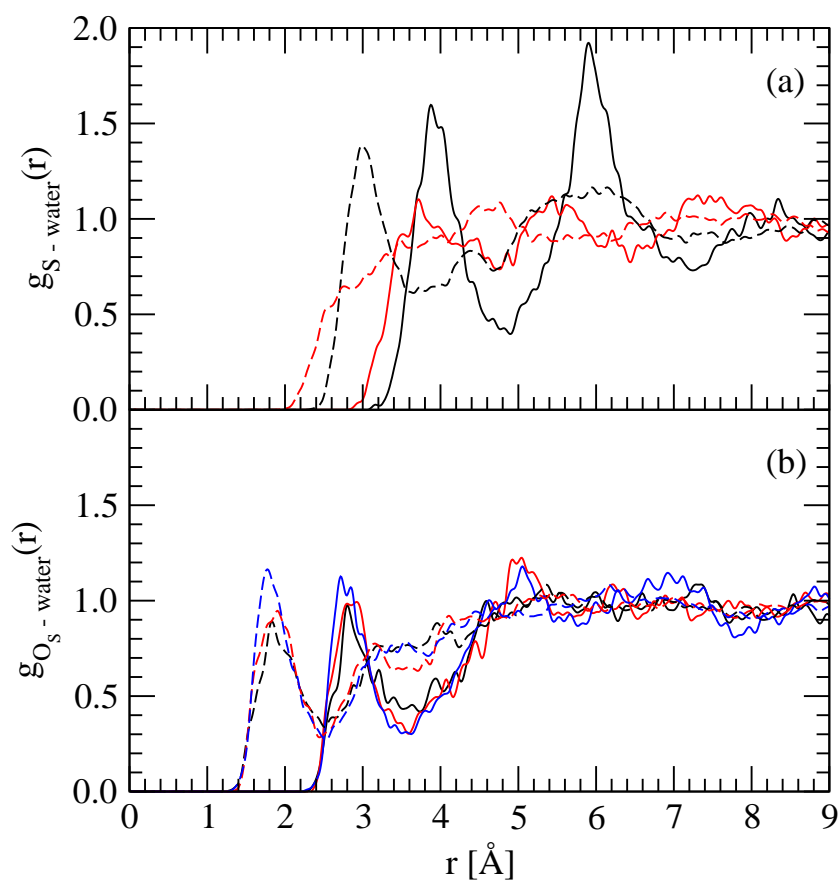


Figure 3.8: The atomic RDF plots of (a) S(1) and S(2) atoms referring to black and red lines, and (b) O(3), O(4) and O(5) atoms presenting with black, red and blue lines; solid and dashed lines refer to the RDFs for the O and H atoms of water, respectively

Interestingly, from the Figure 3.8a, the atomic RDFs of the center S(1) atom showing clearly hydration structures are complicated by the fact that center atom located inside the molecule is hardly interact with water because it is surrounded with the other terminated atoms [77]. When we analyzed deeply in detail and used O_{water} as the center of mass of water molecule to explain the phenomena, we found

Table 3.6: Characteristic values of the radial distribution function $g_{\alpha\beta}(r)$ for each site of $S_2O_3^{2-}$ ion in the hydration shell determined by the QMCF MD simulation

coordinating site	$r_{max}(O_w)^a$	$r_{min}(O_w)^a$	$r_{max}(H_w)^a$	$r_{min}(H_w)^a$	n^a
S(1)	3.88	4.90	3.00	3.66	8.9
S(2)	3.72	3.92	–	3.18	3.5
O(3)	2.80	3.74	1.84	2.50	2.9
O(4)	2.92	3.58	1.90	2.44	2.6
O(5)	2.72	3.62	1.78	2.50	2.7
Surface	2.82	3.82	1.82	2.42	9.2

^a r_{max} and r_{min} are the distances of the maximum and minimum of $g_{\alpha\beta}(r)$ for the hydration shell in Å, and n is the averaged coordination numbers of the shell, respectively.

that the RDFs of S(1) is not the hydration shell by itself. The distance 4.90 Å of the boundary (r_{min}) of S(1) \cdots O_{water} RDF may correspond to the direct sum of distances between the S(1) – O bond (~ 1.5 Å) and its hydration boundary of oxygen site O_S \cdots O_{water} (~ 3.6 Å), indicating that the first band of this RDF coincides with the hydration spheres of oxygen sites. And the RDFs of the terminated S(2) atom are also unusual band. Remarkably, the RDF of S(2) \cdots H_{water} presented in Figure 3.8a shows the broadband of the hydration shell without the characteristic of the peak due to the hydrophobic property of the S – S bond as proven in Figure 3.5, and this results in the difficulty to indicate the boundary of the atomic hydration sphere of the S(2) \cdots O_{water} RDF. When we used the same criterion with the other atoms to make a decision on the band position at the lowest point, the RDF displayed the significant minimum at the location of 4.76 Å. However, this distance is larger than the size of thiosulfate ion and also includes the hydration shell of the other sites. Thus, we reconsidered the hydration sphere of the S(2) site and defined the first minimum at 3.92 Å adjacent to the highest peak as the boundary of S(2) \cdots O_{water} RDF. The boundary of S(2) \cdots H_{water} RDF is also ambiguous, but we locate its boundary in order to use in CND in the next analysis section by seeking the position giving the same integration number as obtained from the boundary of the S(2) \cdots O_{water} RDF which is at 3.18 Å. Displayed in Figure 3.8b, the hydration spheres of all oxygen atoms within the thiosulfate ion (O_s) are similar corresponding to a slight variation of S(1) \cdots O_s lengths as mentioned above. Moreover, the minima of the hydration shells of all atomic RDFs in Figure 3.8 are above the baseline representing the exchanges of the water ligand between the hydration shells and bulk solution.

Coordination Number Distributions (CNDs)

The coordination number distribution (CND) shows the spread of the amount of water coordinating with the solute. To evaluate the CND, the boundary position of the atomic hydration shell obtained from its (site) $\cdots O_{\text{water}}$ RDF is employed to assign the edge to count the number of water molecules as radius from each site. The procedure for the evaluation of atomic CND counts the number of water molecules, occurring within the sphere constructed by the boundary from the RDF. The coordination number (CN or n) relates to the total number of water molecules interacting with the solute throughout the simulation time. It can be obtained from the arithmetic mean of CND and presented in the last column of Table 3.6. As described in the last section, the RDF of S(1) affected from water interacting with neighbouring oxygen atoms contains water in the atomic hydration shells of three oxygen atoms, therefore, the coordination number of S(1) (8.9) is close to the direct sum of the CN values of three oxygen atoms (8.2). The higher CN of S(1) than the total value of three oxygen atoms resulted from a large diameter of hydration sphere of the S(1) atom obtained from the distance to its boundary includes some water molecules from some part of the hydration sphere of S(2) atom. However, the direct sum of CNs misleads the interpretation of the CN of solute via the over-counting of water molecules within the intersection of atomic hydration spheres [84], indicating the location of waters in the intersection of the atomic hydration spheres.

3.3.2 The Molecular Hydration Shell

To study the properties of hydration shell of the solute in aqueous solution, the molecular approach is applied to evaluate the RDFs and CN for the thiosulfate ion. The molecular RDF provides the possibility to find water molecules within the isotropic molecular domain. It is obtained as the distance from the molecular surface of solute molecule, calculated by the combination of all atomic hydration shells constructed from the union of spheres having the identical radii [55]. The coordinating site is assigned by the shortest distance among the values obtained from the oxygen of water and each site within the thiosulfate ion. The evaluation of

molecular RDFs with or without the inclusion of S(1) atom gives the same distributions due to the weak interaction with solvent in comparison with the terminated S(2) and O_S atoms, denoting a negligible role of it in the molecular hydration shell. Therefore, we interest in the interactions of water molecules and four coordinating sites: terminated sulfur, S(2), and oxygen, O(3) – O(5) or O_S, atoms of thiosulfate anion. The molecular domain mentioned in a further analysis will exclude the S(1) atom. The molecular RDFs of the thiosulfate ion demonstrated in Figure 3.9a shows a well-defined hydration structure. The positions of the first peak (r_{max}) and its boundary (r_{min}) of the molecular hydration shells of the thiosulfate ion are also listed in Table 3.6 in the last row labeled as surface. The distance between the first peak of (molecular) \cdots O_{water} (2.82 Å) and (molecular) \cdots H_{water} (1.82 Å) RDFs is 1.00 Å corresponding to the average length of O – H bonds (0.98 ± 0.03 Å) within water molecules located in the molecular hydration shell, confirming the orientation of water molecules using one hydrogen atom to coordinate with the ion.

The molecular CND is evaluated and displayed in Figure 3.9b with the molecular domain constructed by applying the boundary obtained from the atomic RDFs of each site of the thiosulfate ion [55]. All possible coordination numbers (CNs) of thiosulfate are in the range of 6 to 12 with a dominant value of 9. The average coordination number (CN) from the molecular RDFs and CND are also reported in Table 3.6. The direct summation of average atomic CNs for the coordinating sites (11.7) excluding the one of S(1) atom is higher than the molecular CN (9.2), differing by 2.5 molecules. The different value indicates that some water molecules locate in the intersection volume of the atomic hydration spheres, referring a water molecule can interact with more than one site.

The factors effecting on the molecular coordination number are described below.

1. The different property of atom

The molecular CN of thiosulfate (9.2) is slightly less than the value of sulfate ion (10.4) [76] consistent with the hydrophobic properties of S – S bond within the thiosulfate ion.

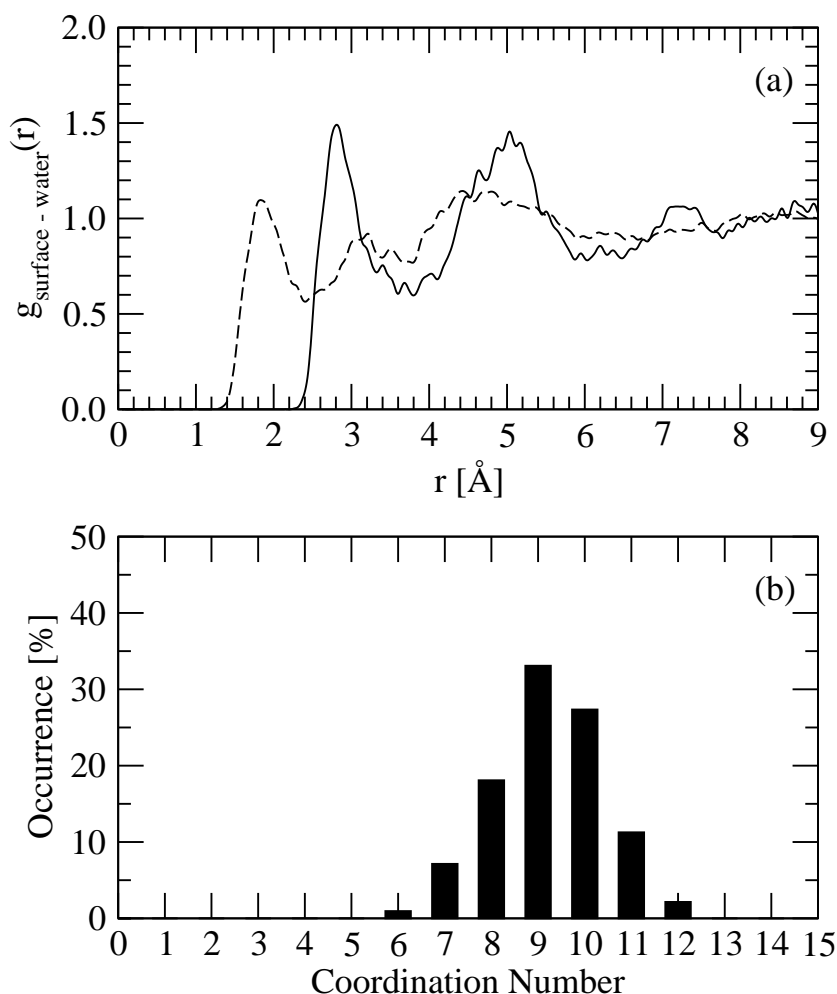


Figure 3.9: (a) Molecular RDF plots of $\text{S}_2\text{O}_3^{2-}$ ion obtained from the QMCF MD simulation evaluated by means of the molecular domain; solid and dashed lines refer to the RDF for the O and H atoms of water, respectively. (b) The molecular hydration shell coordination number distribution of the ion

2. Charge of the molecule

The molecular CN of sulfonate ion with a single negative charge is 6.6 [75], presenting weaker interaction and hydration shell than the thiosulfate ion by the effect of charge on the strength of the molecular hydration shell less interacting with solvent water molecules.

The molecular CN of thiosulfate in this research is less than the hydration number obtained from the ultrasonic velocity data which is 13 water molecules located in the hydration shell of the ion [31]. Actually, we got the similar value of 12.9 if

we utilized the boundary for the S(2) hydration sphere at 4.76 Å as the first time, but it is too large atomic hydration sphere as above explanation. This leads to the conclusion that the evaluated CN method is sensitive with the selection of the boundary for the atomic hydration sphere, therefore, we also calculate an actual CN with a precise approach in the next section.

3.3.3 Actual Coordination Number

The water molecules interacting around the solute via the hydrogen bond (H-bond) can induce other water molecules to come closer for interacting and binding via H-bond as network resulting to the over value of real coordination number. There are two groups of water molecules in the hydration shell: water molecules directly interact with solute and the others, called extra water molecules, interact with the former kind of water in the first layer. We can calculate the number of the extra water in the H-bond network located between the molecular hydration shell and bulk by the different value between the molecular CN and the number of actual contact. The actual contact number can be obtained by counting the number of hydrogen bond determined from the parameters (bond distance and angle) of a suitable orientation of a water molecule to form the H-bond in accordance with the geometric criterion. This depends on the cutoff parameters in analogy to water–dimethyl sulfoxide [85] and our previous studies [75,77,80] denoted by $R_{(1)(2)}^{(c)}$, which the first letter is labelled as an atom of thiosulfate and the second one is labelled as an atom of water molecule. The cutoff distances $R_{OO}^{(c)}$ and $R_{OH}^{(c)}$ for each oxygen site of thiosulfate correspond to the boundary of the atomic hydration spheres obtained from (site) \cdots O_{water} and (site) \cdots H_{water} RDFs respectively. We also define the cutoff distances of S(2), namely the $R_{SO}^{(c)}$ and $R_{SH}^{(c)}$, with the boundary of the atomic hydration sphere from the S(2) \cdots O_{water} RDF at 3.92 for the former, while the corresponding S(2) \cdots H_{water} RDF for the latter is 3.18 Å. The difference referring to O – H is too short to form and determine the suitable H-bond. According to the molecular RDFs, the different distance between the first peak of (molecular) \cdots O_{water} and (molecular) \cdots H_{water} (1.00 Å) suggests a co-linear arrangement for O – H bond within a water molecule to form a H-bond with a coordinating site of thiosulfate; thus, we specify the $R_{SH}^{(c)}$

at 2.92 Å. The angle $\varphi^{(c)}$, another parameter, is set as 30° [85] at the first time. Table 3.7 lists the average number of H-bonds for each site and the molecular hydration (surface) of the thiosulfate ion. The H-bonds of the surface is the average value of the summation of all H-bonds in each time step over the simulation period.

Table 3.7: Average number of hydrogen bonds for each coordinating site and molecular hydration of $S_2O_3^{2-}$ ion in the simulation period

coordinating site	H-bonds
S(2)	1.4 ± 0.8
O(3)	1.7 ± 0.7
O(4)	1.7 ± 0.7
O(5)	2.0 ± 0.7
surface	6.8 ± 1.3

The equivalence between the direct sum of each site and the surface values with the ratio 1:1 for the H-bond formation between the water molecule and the coordinating site proves that the actual contacts are 6.8 obtained from the average H-bond of molecular surface and the extra water molecules are 2.4 ($9.2 - 6.8$) obtained from the difference of the molecular coordination number (CN) and the number of actual contact. The extra water molecules are located in the molecular hydration without having the interaction and forming H-bond with the ion directly. The previous study reported the actual CN of nitrate as 5.2 [80], indicating a weaker interaction with its molecular hydration than the thiosulfate ion as same as the conclusion from the ultrasonic velocity experiment [31]. The actual CN indicates that the thiosulfate has a stronger interaction with the molecular hydration than the sulfonate ion (with the value of 5.0) [75], reflecting the influence of charge on this incidence. We also reinvestigate the actual CN for the sulfate ion [76] with the same procedure and obtain the value of 7.7 ± 1.5 showing a stronger interaction with its molecular hydration than the thiosulfate ion, corresponding with the consisting of the hydrophobic S – S bond in the latter ion. The actual contact number compared with the other ions is agree with the molecular CN as explained before.

3.3.4 Mean Residence Time (MRT)

The further dynamical property of water molecules hydrating the thiosulfate ion within the hydration shell is investigated by means of the ligand mean residence time (MRT), calculated by the direct method [56]. This method employs 2 kinds of the average number of water molecules within the hydration shell during the simulation period evaluated by the number of exchange events with two time parameters ($t^* = 0.0$ and 0.5 ps) corresponding to all displacements and sustainable exchange events, respectively [57]. These t^* parameters are set to use as a basic measurement to count all the number of the water molecules and the exchange processes occurring in the interested period. The $t^* = 0.0$ ps is defined as the minimum duration of a ligand displacement from its original shell to account for an exchange process. This parameter counts all exchange attempts whenever water molecules come in and out of the boundary of the hydration shell. While, the $t^* = 0.5$ ps is set in accordance with the average of H-bond life time from $\text{H}_2\text{O} \cdots \text{H}_2\text{O}$ interaction of pure water. This parameter is used as a criterion to determine water molecules (ligands) having long time interaction with the solute ion. The standard relaxation time utilized in the direct method with $t^* = 0.5$ ps leads to the MRT of water ligands at the coordinating sites, while the hydrogen bond lifetimes can be estimated with $t^* = 0.0$ ps [56,84]. Table 3.8 lists all MRT values for all coordinating sites and molecular hydration shell for the thiosulfate ion, compared with the data of pure water simulations [56,86].

The number of involved ligands (N_{inv}) represents the number of all water molecules involving to coordinate with the evaluated site in the criterion of t^* , while the number of accounted exchange events (N_{ex}) accumulates the exchange process of all water molecules of N_{inv} throughout the simulation period. The summations of all number of water molecules (N_{inv}) counted for individual exchange processes of all coordinating sites of $t^* = 0.0$ ps ($32 + 23 + 24 + 24 = 103$) and $t^* = 0.5$ ps ($10 + 13 + 14 + 9 = 46$) are higher than those counted for the molecular hydration shell (45 and 28 respectively). Furthermore, the summations of the number of attempted and lasting exchange processes (N_{ex}) of individual atoms evaluated at $t^* = 0.0$ ps ($285 + 151 + 106 + 105 = 647$ events) and at $t^* = 0.5$ ps ($25 + 26 + 21 + 20 = 92$ events) are also greater than the 315 and 46 events, respectively, counted by the molecular ap-

Table 3.8: Mean ligand residence time τ (ps), number of accounted ligand exchange events N and total number of processes needed for one successful water exchange R_{ex} obtained from the QMCF MD simulation

	$t^* = 0.0$ ps			$t^* = 0.5$ ps			R_{ex}^d
	N_{inv}^a	$N_{ex}^{0.0}/10$ ps ^b	$\tau_D^{0.0c}$	N_{inv}^a	$N_{ex}^{0.5}/10$ ps ^b	$\tau_D^{0.5c}$	
S(2)	32	285	0.07	S ₂ O ₃ ²⁻			11.4
O(3)	23	151	0.20	10	25	1.47	5.8
O(4)	24	106	0.25	13	26	1.17	5.0
O(5)	24	105	0.26	14	21	1.26	5.2
Surface	45	315	0.28	9	20	1.37	6.8
				28	46	2.03	
				Pure water			
H ₂ O ^e		269 [56]	0.2 [56], 0.33 [86]		24 [56]	1.7 [56], 1.51 [86]	11.2 [56]
H ₂ O		131 ^f	0.2 ^f , 0.55 [57]		20 ^f	1.3 ^f	6.5 ^f

^aNumber of ligand involved in the MRT evaluation according to the value of t^* .

^bNumber of accounted exchange events per 10 ps lasting at least 0.0 and 0.5 ps, respectively.

^cMean residence time determined by the direct method [56] in picoseconds.

^dAverage number of processes needed for one successful ligand exchange.

^eValues obtained from a QM/MM-MD simulation of pure water [56,86] in picoseconds.

^fUnpublished results: values obtained from a QMCF MD simulation of pure water in picoseconds.

proach which avoids counting water molecules within the intersection of individual atomic hydration spheres. Showing that the summations from the coordinating sites are higher than those from the molecular surface, these values again prove that there are some water molecules locating in the intersection volume of the atomic hydration spheres.

At the time which the real exchange processes happen, the exchange events at $t^* = 0.5$ ps of the total atomic $N_{ex}^{0.5}$ (92 events) and the molecular $N_{ex}^{0.5}$ (46 events), the over value from the surface ($92 - 46 = 46$ events) is suggested to be the number of migrations of water molecules between the coordinating sites of thiosulfate ion as proven in the next section, despite $N_{ex}^{0.5}$ of the surface (46 events), which is the events of water molecules migrating between the molecular surface of the ion and bulk. This number of the migration events within the ion is equal to its molecular value representing the confined waters within the molecular hydration shell and reflecting a longer MRT of the molecular hydration than each coordinating site.

Considering the value of S(2), $N_{ex}^{0.0}$ (285 events) is greater than $N_{ex}^{0.5}$ (25 events). The former shows many events of the short time interaction with the ion, while the latter represents lower events of the longer time interaction. This demonstrates that water molecules do not situate close to S(2), indicating the hydrophobic property of

the S – S bond. And the $\tau_D^{0.0}$ of S(2) site also indicates a remarkably short lifetimes for the formation of H-bonds with water molecules, proving the hydrophobic property of this S – S bond. It is introduced a peculiar property by the most MRT value for this site comparing to other atomic sites, caused by the confined water molecules within the intersection volumes of atomic hydration spheres around the S(2) site.

The $\tau_D^{0.5}$ of the molecular surface of the thiosulfate ion is greater than the pure water, demonstrating that the ion interacts with water molecules via H-bond better and longer time than the $H_2O \cdots H_2O$ interaction with themselves. Moreover, the molecular MRT reveals a strong hydration structure than the pure water; thus, we classify the thiosulfate ion as a structure-maker consisting of three hydrophilic S – O and one hydrophobic S – S bonds. The weak interaction between the S(2) site with a water molecule suggests that it is the active site to interact with other species in solutions, supporting to the characterizations in many chemical reactions [23–25,87].

The number of processes needed for one successful water exchange is called R_{ex} , which is the ratio of $N_{ex}^{0.0}$ to $N_{ex}^{0.5}$ as shown in the equation (2.20). This value presents a complexity of the exchange process, according to the significant difference between the atomic and molecular R_{ex} especially for the S(2) site. The N_{ex} values of the atomic sites count all exchange events from each site to both the other sites and bulk according with intra- and inter-molecular hydration shell, respectively. The R_{ex} of each site shows only the ratio of events referable to move in or out of that site, but it can not manifest where the water will go or come from. Besides, N_{ex} of the molecular surface counts only the exchange events between the surface and bulk. To investigate about migration between sites inside the molecular hydration shell, therefore, we have to study from N_{ex} counting from only the exchanges among sites by subtraction N_{ex} of the surface from the summation of all atomic sites, resulting to $N_{ex}^{0.0} = 647 - 315 = 332$ and $N_{ex}^{0.5} = 92 - 46 = 46$. Thus, $R_{ex} = \frac{N_{ex}^{0.0}}{N_{ex}^{0.5}} = \frac{647-315}{92-46} = \frac{332}{46} = 7.2$. The R_{ex} for the interchanging of the coordinating sites within the molecular hydration shell is 7.2 close to the value of molecular hydration (6.8), presenting an analogy of exchanging rate between intra- and inter-molecular hydration shell for water molecules, respectively.

3.3.5 Dynamics of the Water Molecules

The dynamical data of all atoms within the system were being collected during the simulation. The visualization of the hydration shell during the simulation period provides an insight to understand the motion of water molecules around the solute. We investigated via superimposed trajectories with 3D alignment, and found that some water molecules migrate within the hydration shell and even some come in and out of the boundary. In here, we represent only one selected water molecule moving within the molecular hydration shell throughout the simulation time. This water shows the migration between the coordinating sites and also the location in the intersection volume. Figure **3.10** illustrates the confined water molecule within simultaneous atomic hydration spheres in some period of the simulation time, presented in both distances plot from each coordinating site and the superimposed trajectories with 3D alignment based on the contravariant transformation [75].

Exhibiting in the Figure **3.10**, the water moves all the time but it is mostly close to the distance around 3 Å which is consistent with the $r_{max}(O_w)$ values as reported in the Section 3.3.1 (RDFs). These values in the Table **3.6** illustrate the average distance (ca. 3.0 Å) from all configurations in the simulation between site of thiosulfate and oxygen atom of water to form H-bond during the simulation time.

The coordinating site can be determined by the nearest distance of the water from each site in the Figure **3.10a**. At the beginning this water locates near and interacts with O(3) and then rapidly changes the coordinating site from O(3) to S(2) at 0.3 ps and relapses to O(3) again at 1.5 ps, whereas it is far from the other two oxygen sites during the simulation time as proven in Figure **3.10b**. In this time region, this selected water molecule shows the migration between the coordinating sites within the molecular hydration shell. The distances of the water from both coordinating sites in the time period during 3.2 to 5.3 ps are close demonstrating that the water stays close to both coordinating sites. Therefore, this selected water molecule clearly presents the location in the intersection volume of the atomic hydration spheres; however, the coordinating site for the water in this period is the O(3) site by the basis of molecular hydration shell as mentioned above.

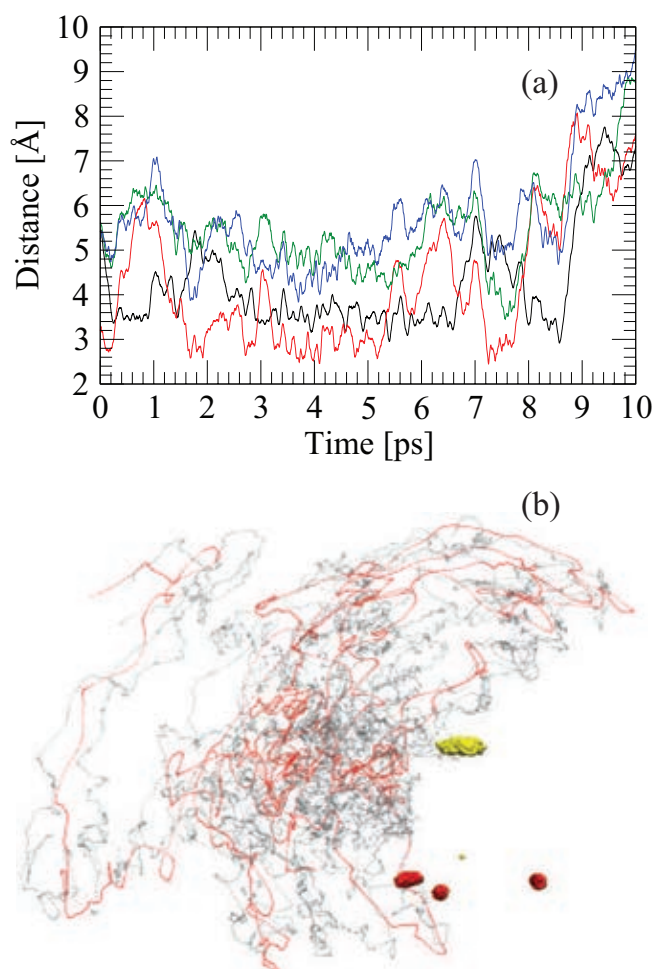


Figure **3.10**: (a) Distances plot of the selected water molecule evaluated from S(2) (black solid line), O(3) (red solid line), O(4) (green solid line), and O(5) (blue solid line) sites as a function of time during the QMCF MD simulation period. (b) All superimposed trajectories for the coordination of the selected water with 3D alignment. The yellow and red spheres are sulfurs and oxygens of $S_2O_3^{2-}$, respectively, red and gray dots are the oxygen and hydrogens of the water.

The location of water molecules in the intersection volume results to the overestimated values of the atomic analysis *e.g.* atomic RDFs, atomic CNDs and atomic MRTs. The data of this water molecule clarified an overestimation of atomic MRT for the S(2) site and present the migration of a water molecule within the molecular hydration shell among coordinating sites. The atomic MRTs of oxygen atoms indicate an inclusion of these sites in H-bonds network of surrounding waters.

CHAPTER IV

CONCLUSION

The QMCF MD simulation is a powerful tool to study the structural and dynamical properties of a solute dissolved in the water as a solution. The fundamental properties of the thiosulfate ion in the aqueous solution with explicit water molecules were studied by creating the cubic box with the periodic boundary conditions [44] to make the dilute solution having the density as the water. The optimized geometries of thiosulfate ion from various theoretical levels indicated that the inclusion of implicit water model reduces all bond lengths within the ion, specifying a role of water molecules in the explicit way. The structural parameters from the simulation result represented a significant effect of water on the S – S bond. This bond shows a hydrophobic property as it presents a shorter length when a water molecule comes close to the terminated sulfur or S(2) atom, having a similar property to the S – H bond within the sulfonate ion [75]. This situation reflected in a splitting peaks of the $\nu(\text{SS})$ spectrum. The atomic RDFs present a difficulty to clarify a hydration structure for the thiosulfate ion, while the molecular RDFs indicates a clearly molecular hydration shell and the orientation of water molecules pointing a hydrogen to interact with the coordinating site. The evaluation of CNs is sensitive to the selection of the atomic hydration spheres; thus, the number of actual contacts separated from the CN by the criterion of the H-bonds formation was respected. The greater number of actual contacts for the thiosulfate (6.8) than nitrate ion (5.2) [80] indicates the stronger hydration structure of the former than the latter, supporting the experimental comparison of the hydration number for both ions [31]. A further investigation on the peculiar atomic MRT results of S(2) confirms the hydrophobicity of this site while the oxygen sites exhibit the stronger interaction with the water molecules within the hydration shell. These results suggest the steric effects of water molecules within the hydration shell protecting the oxygen sites in aqueous solutions, and leave the active S(2) site readily involving in chemical reactions.

REFERENCES

- [1] D. Muir, M. Aylmore In *Developments in mineral processing*; M. Adams, Ed.; Elsevier: Amsterdam, 2005; Vol. 15; chapter 22, pages 541–560.
- [2] G. Senanayake *Role of copper(II), carbonate and sulphite in gold leaching and thiosulphate degradation by oxygenated alkaline non-ammoniacal solutions* Miner. Eng., **2005**, *18*, 409–426.
- [3] D. Feng, J. Deventer *The effect of iron contaminants on thiosulphate leaching of gold* Miner. Eng., **2010**, *23*, 399–406.
- [4] D. Feng, J. Deventer *The role of amino acids in the thiosulphate leaching of gold* Miner. Eng., **2011**, *24*, 1022–1024.
- [5] T. H. James In ; T. H. James, Ed.; MacMillan: New York, 1977; chapter 16.
- [6] D. Gonnissen, S. Vandeputte, A. Hubin, J. Vereecken *Investigation of the mechanism of silver deposition from thiosulphate solutions by means of ac impedance measurements and surface-enhanced raman spectroscopy* Electrochim. Acta, **1996**, *41*, 1051–1056.
- [7] P. Wang, Y. Yuan, X. Jing, G. Zhu *Amperometric determination of thiosulfate at a surface-renewable nickel(II) hexacyanoferrate-modified carbon ceramic electrode* Talanta, **2001**, *53*, 863–869.
- [8] W. Simons, D. Gonnissen, A. Hubin *Study of the initial stages of silver electrocrystallisation from silver thiosulphate complexes Part I: Modelling of the silver nuclei formation during the induction period* J. Electroanal. Chem., **1997**, *433*, 141–151.
- [9] D. Gonnissen, W. Simons, A. Hubin *Study of the initial stages of silver electrocrystallisation from silver thiosulphate complexes Part II. Analysis of current transients* J. Electroanal. Chem., **1997**, *435*, 149–155.
- [10] B. Lui, Z. Ma, K. Li *Sculpturing effect of sodium thiosulfate in shape transformation of silver nanoparticles from triangular nanoprisms to hexagonal nanoplates* J. Nanosci. Nanotechnol., **2011**, *11*, 5001–5006.

- [11] M. Hensel, A. P. Hinsley, T. Nikolaus, G. Sawers, B. C. Berks *The genetic basis of tetrathionate respiration in Salmonella typhimurium* Mol. Microbio., **1999**, *32*, 275–287.
- [12] F. H. Müller, T. M. Bandejas, T. Urich, M. Teixeira, C. M. Gomes, A. Kletzin *Coupling of the pathway of sulphur oxidation to dioxygen reduction: characterization of a novel membrane-bound thiosulphate:quinone oxidoreductase* Mol. Microbio., **2004**, *53*, 1147–1160.
- [13] N.-U. Frigaard, C. Dahl Vol. 54 of *Advances in microbial physiology*; Academic Press, 2008; pages 103–200.
- [14] D. Sullivan, J. Havlin *Thiosulfate inhibition of urea hydrolysis in soils: tetrathionate as a urease inhibitor* Soil Sci. Soc. Am. J., **1992**, *56*, 957–960.
- [15] R. Goos *Identification of ammonium thiosulfate as a nitrification and urease inhibitor* Soil Sci. Soc. Am. J., **1985**, *49*, 232–235.
- [16] J. Gan, S. Yates, J. Becker, D. Wang *Surface amendment of fertilizer ammonium thiosulfate to reduce methyl bromide emission from soil* Environ. Sci. Technol., **1998**, *32*, 2438–2441.
- [17] J. Gan, J. O. Becker, F. F. Ernst, C. Hutchinson, J. A. Knuteson, S. R. Yates *Surface application of ammonium thiosulfate fertilizer to reduce volatilization of 1,3-dichloropropene from soil* Pest. Manag. Sci., **2000**, *56*, 264–270.
- [18] F. A. Miller, C. H. Wilkins *Infrared spectra and characteristic frequencies of inorganic ions* Anal. Chem., **1952**, *24*, 1253–1294.
- [19] V. E. Steger, I. C. sowie A. Fadini *Das Infrarotspektrum von natriumchlorosulfat und die kraftkonstanten der Ionen $[SO_3Cl]^-$, $[SO_3F]^-$ und $[SO_3S]^{2-}$* Z. Anorg. Allg. Chem., **1967**, pages 225–336.
- [20] J. Haigh, P. Hendra, A. Rowlands, I. Degen, G. Newman *Raman spectroscopy of thiosulphates* Spectrochim. Acta, Part A, **1993**, *49*, 723–725.
- [21] J. Church, D. Evans *A spectroscopic investigation into the reaction of sodium tetrathionate with cysteine* Spectrochim. Acta, Part A, **2008**, *69*, 256–262.

- [22] L. Rintoul, K. Crawford, H. F. Shurvell, P. M. Fredericks *Surface-enhanced raman scattering of inorganic oxoanions* Vib. Spectrosc., **1997**, *15*, 171–177.
- [23] R. Narayanan, M. A. El-Sayed *Raman studies on the interaction of the reactants with the platinum nanoparticle surface during the nanocatalyzed electron transfer reaction* J. Phys. Chem. B, **2005**, *109*, 18460–18464.
- [24] R. A. Bryce, J. M. Charnock, R. A. D. Patrick, A. R. Lennie *EXAFS and density functional study of gold(I) thiosulfate complex in aqueous solution* J. Phys. Chem. A, **2003**, *107*, 2516–2523.
- [25] B. E. Etschmann, J. R. Black, P. V. Grundler, S. Borg, D. Brewé, D. C. McPhail, L. Spiccia, J. Brugger *Copper(I) speciation in mixed thiosulfate-chloride and ammonia-chloride solutions: XAS and UV-Visible spectroscopic studies* RSC Adv., **2011**, *1*, 1554–1566.
- [26] A. Nishimoto, D. Y. Zhang *Hypervalency in sulfur ab initio and DFT studies of the structures of thiosulfate and related sulfur oxyanions* Sulfur Lett., **2003**, *26*, 171–180.
- [27] M. L. McKee *Computational study of the mono- and dianions of SO_2 , SO_3 , SO_4 , S_2O_3 , S_2O_4 , S_2O_6 , and S_2O_8* J. Phys. Chem., **1996**, *100*, 3473–3481.
- [28] A. I. Boldyrev, J. Simons *Isolated SO_4^{2-} and PO_4^{3-} anions do not exist* J. Phys. Chem., **1994**, *98*, 2298–2300.
- [29] B. M. Rode, T. S. Hofer, B. R. Randolph, C. F. Schwenk, D. Xenides, V. Vchirawongkwin *Ab initio quantum mechanical charge field (QMCF) molecular dynamics: a QM/MM-MD procedure for accurate simulations of ions and complexes* Theor. Chem. Acc., **2006**, *115*, 77–85.
- [30] T. S. Hofer, A. B. Pribil, B. R. Randolph, B. M. Rode In *Combining quantum mechanics and molecular mechanics. Some recent progresses in QM/MM methods*; J. R. Sabin, E. Brändas, Eds., Vol. 59 of *Advances in quantum chemistry*; Academic Press, 2010; pages 213–246.

- [31] N. Rohman, S. Mahiuddin *Concentration and temperature dependence of ultrasonic velocity and isentropic compressibility in aqueous sodium nitrate and sodium thiosulfate solutions* J. Chem. Soc., Faraday Trans., **1997**, 93, 2053–2056.
- [32] P. G. Taylor, C. A. Beevers *The crystal structure of sodium thiosulphate pentahydrate* Acta Cryst., **1952**, 5, 341–344.
- [33] M. Nardelli, G. Fava *The crystal structure of barium thiosulphate monohydrate* Acta Cryst., **1962**, 15, 477–484.
- [34] L. A. Manojlović-Muir *A neutron diffraction study of barium thiosulphate monohydrate, $BaS_2O_3 \cdot H_2O$* Acta Cryst., **1975**, B31, 135–139.
- [35] A. A. Uraz, N. Armağan *An X-ray diffraction study of sodium thiosulphate pentahydrate, $Na_2S_2O_3 \cdot 5H_2O$* Acta Cryst., **1977**, B33, 1396–1399.
- [36] G. C. Lisensky, H. A. Levy *Sodium thiosulfate pentahydrate: a redetermination by neutron diffraction* Acta Cryst., **1978**, B34, 1975–1977.
- [37] N. Armağan *Rigid-body motion of the $S_2O_3^{2-}$ group in thiosulphates* Acta Cryst., **1983**, A39, 647–650.
- [38] Y. Elerman, J. W. Bats, H. Fuess *Deformation density in complex anions. IV. Magnesium thiosulfate hexahydrate, $MgS_2O_3 \cdot 6H_2O$* Acta Cryst., **1983**, C39, 515–518.
- [39] S. T. Teng, H. Fuess, J. W. Bats *Refinement of sodium thiosulfate, $Na_2S_2O_3$, at 120 K* Acta Cryst., **1984**, C40, 1785–1787.
- [40] W. Hesse, B. Leutner, K.-H. Böhn, N. P. C. Walker *Structure of a new sodium thiosulfate hydrate* Acta Cryst., **1993**, C49, 363–365.
- [41] S. M. Prasad, A. Rani *Rerefinement of sodium thiosulfate pentahydrate* Acta Cryst., **2001**, E57, i67–i69.
- [42] P. Held, L. Bohatý *Calcium and strontium thiosulfate, $CaS_2O_3 \cdot 6H_2O$ and $SrS_2O_3 \cdot 5H_2O$* Acta Cryst., **2004**, C60, i97–i100.
- [43] S. Alvarez, V. Tabacik, J. Casabo *J. Mol. Struc.*, **1985**, 130, 235–243.

- [44] M. Allen, D. Tildesley; Oxford University Press: New York, 1991.
- [45] A. Warshel, M. Levitt *Theoretical studies of enzymic reactions: dielectric, electrostatic and steric stabilization of the carbonium ion in the reaction of lysozyme* J. Mol. Bio., **1976**, *103*, 227–249.
- [46] M. J. Field, P. A. Bash, M. Karplus *A combined quantum mechanical and molecular mechanical potential for molecular dynamics simulations* J. Comput. Chem., **1990**, *11*, 700–733.
- [47] J. Gao *Potential of mean force for the isomerization of DMF in aqueous solution: a Monte Carlo QM/MM simulation study* J. Am. Chem. Soc., **1993**, *115*, 2930–2935.
- [48] D. Bakowise, W. Thiel *Hybrid models for combined quantum mechanical and molecular mechanical approaches* J. Phys. Chem., **1996**, *100*, 10580–10594.
- [49] B. R. Brooks, R. E. Bruccoleri, B. D. Olafson, B. D. States, S. Swaminathan, M. Karplus *CHARMM: a program for macromolecular energy, minimization, and dynamics calculations*. J. Comput. Chem., **1983**, *4*, 187–217.
- [50] H. J. C. Berendsen, J. P. M. Postma, W. F. van Gunsteren, A. DiNola, J. R. Haak *Molecular dynamics with coupling to an external bath* J. Chem. Phys., **1984**, *81*, 3684–3690.
- [51] T. H. Dunning, Jr., P. J. Hay In *Modern theoretical chemistry: methods of electronic structure theory*; H. F. Schaefer III, Ed.; Plenum Press: New York, 1977; Vol. 3; chapter 1, pages 1–27.
- [52] T. H. Dunning, Jr. *Gaussian basis functions for use in molecular calculations. I. Contractions of (9s5p) atomic basis sets for the first-row atoms* J. Chem. Phys., **1970**, *53*, 2823–2833.
- [53] F. H. Stillinger, A. Rahman *Revised central force potentials for water* J. Chem. Phys., **1978**, *68*, 666–670.
- [54] P. Bopp, G. Jansc , K. Heinzinger *An improved potential for non-rigid water molecules in the liquid phase* Chem. Phys. Lett., **1983**, *98*, 129–133.

- [55] S. Vchirawongkwin, V. Vchirawongkwin *Evaluation of molecular radial distribution function and solvent-excluded volume with the numerical integration of the union of spheres* *Comput. Theor. Chem.*, **2011**, 974, 26–30.
- [56] T. S. Hofer, H. T. Tran, C. F. Schwenk, B. M. Rode *Characterization of dynamics and reactivities of solvated ion by ab initio simulations* *J. Comput. Chem.*, **2004**, 25, 211–217.
- [57] A. J. Lock, S. Woutersen, H. J. Bakker *Ultrafast energy equilibration in hydrogen-bonded liquids* *J. Phys. Chem. A*, **2001**, 105, 1238–1243.
- [58] P. Bopp *A study of the vibrational motions of water in an aqueous CaCl_2 solution* *Chem. Phys.*, **1986**, 106, 205–212.
- [59] P. Mark, L. Nilsson *Structure and dynamics of the TIP3P, SPC, and SPC/E water models at 298 K* *J. Phys. Chem. A*, **2001**, 105, 9954–9960.
- [60] W. L. Jorgensen, J. Chandrasekhar, J. D. Madura, R. W. Impey, M. L. Klein *Comparison of simple potential functions for simulating liquid water* *J. Chem. Phys.*, **1983**, 79, 926–935.
- [61] E. Neria, S. Fischer, M. Karplus *Simulation of activation free energies in molecular systems* *J. Chem. Phys.*, **1996**, 105, 1902–1921.
- [62] H. J. C. Berendsen, J. P. M. Postma, W. F. van Gunsteren, J. Hermans In *Intermolecular forces*; B. Pullman, Ed., Vol. 14; Dordrecht Reidel, 1981; pages 331–342.
- [63] C. D. Berweger, W. F. van Gunsteren, F. Müller-Plathe *Force field parametrization by weak coupling. Re-engineering SPC water* *Chem. Phys. Lett.*, **1995**, 232, 429–436.
- [64] H. J. C. Berendsen, J. R. Grigera, T. P. Straatsma *The missing term in effective pair potentials* *J. Phys. Chem.*, **1987**, 91, 6269–6271.
- [65] J.-P. Ryckaert, G. Ciccotti, H. J. Berendsen *Numerical integration of the cartesian equations of motion of a system with constraints: molecular dynamics of n-alkanes* *J. Comput. Phys.*, **1977**, 23, 327–341.

- [66] W. L. Jorgensen *Transferable intermolecular potential functions for water, alcohols, and ethers. Application to liquid water* J. Am. Chem. Soc., **1981**, *103*, 335–340.
- [67] H. L. Lemberg, F. H. Stillinger *Central-force model for liquid water* J. Chem. Phys., **1975**, *62*, 1677–1690.
- [68] A. Rahman, F. H. Stillinger, H. L. Lemberg *Study of a central force model for liquid water by molecular dynamics* J. Chem. Phys., **1975**, *63*, 5223–5230.
- [69] F. H. Stillinger, A. Rahman *Revised central force potentials for water* J. Chem. Phys., **1978**, *68*, 666–670.
- [70] V. Vchirawongkwin, B. M. Rode *Solvation energy and vibrational spectrum of sulfate in water - An ab initio quantum mechanical simulation* Chem. Phys. Lett., **2007**, *443*, 152–157.
- [71] A. Soper, M. Phillips *A new determination of the structure of water at 25°C* Chem. Phys., **1986**, *107*, 47–60.
- [72] W. F. Murphy, H. J. Bernstein *Raman spectra and an assignment of the vibrational stretching* J. Phys. Chem., **1972**, *76*, 1147–1152.
- [73] S. F. Boys, F. Bernardi *The calculation of small molecular interactions by the differences of separate total energies. Some procedures with reduced errors* Mol. Phys., **1970**, *19*, 553–566.
- [74] S. Simon, M. Duran, J. J. Dannenberg *How does basis set superposition error change the potential surfaces for hydrogen-bonded dimers?* J. Chem. Phys., **1996**, *105*, 11024–11031.
- [75] V. Vchirawongkwin, C. Pornpiganon, C. Kritayakornupong, A. Tongraar, B. M. Rode *The stability of bisulfite and sulfonate ions in aqueous solution characterized by hydration structure and dynamics* J. Phys. Chem. B, **2012**, *116*, 11498–11507.
- [76] V. Vchirawongkwin, B. M. Rode, I. Persson *Structure and dynamics of sulfate ion in aqueous solution - an ab initio QMCF MD simulation and large angle X-ray scattering study* J. Phys. Chem. B, **2007**, *111*, 4150–4155.

- [77] V. Vchirawongkwin, C. Kritayakornupong, B. M. Rode *Structural and dynamical properties and vibrational spectra of bisulfate ion in water: a study by ab initio quantum mechanical charge field molecular dynamics* J. Phys. Chem. B, **2010**, *114*, 11561–11569.
- [78] L. Eklund, T. S. Hofer, A. B. Pribil, B. M. Rode, I. Persson *On the structure and dynamics of the hydrated sulfite ion in aqueous solution - an ab initio QMCF MD simulation and large angle X-ray scattering study* Dalton Trans., **2012**, *41*, 5209–5216.
- [79] Gaussian 03, Revision E.01. M. J. Frisch, G. W. Trucks, H. B. Schlegel, G. E. Scuseria, M. A. Robb, J. R. Cheeseman, J. A. Montgomery, T. Vreven, K. N. Kudin, J. C. Burant, J. M. Millam, S. S. Iyengar, J. Tomasi, V. Barone, B. Mennucci, M. Cossi, G. Scalmani, N. Rega, G. A. Petersson, H. Nakatsuji, M. Hada, M. Ehara, K. Toyota, R. Fukuda, J. Hasegawa, M. Ishida, T. Nakajima, Y. Honda, O. Kitao, H. Nakai, M. Klene, X. Li, J. E. Knox, H. P. Hratchian, J. B. Cross, V. Bakken, C. Adamo, J. Jaramillo, R. Gomperts, R. E. Stratmann, O. Yazyev, A. J. Austin, R. Cammi, C. Pomelli, J. W. Ochterski, P. Y. Ayala, K. Morokuma, G. A. Voth, P. Salvador, J. J. Dannenberg, V. G. Zakrzewski, S. Dapprich, A. D. Daniels, M. C. Strain, O. Farkas, D. K. Malick, A. D. Rabuck, K. Raghavachari, J. B. Foresman, J. V. Ortiz, Q. Cui, A. G. Baboul, S. Clifford, J. Cioslowski, B. B. Stefanov, G. Liu, A. Liashenko, P. Piskorz, I. Komaromi, R. L. Martin, D. J. Fox, T. Keith, A. M. A. Laham, C. Y. Peng, A. Nanayakkara, M. Challacombe, P. M. W. Gill, B. Johnson, W. Chen, M. W. Wong, C. Gonzalez, J. A. Pople.
- [80] V. Vchirawongkwin, C. Kritayakornupong, A. Tongraar, B. M. Rode *Symmetry breaking and hydration structure of carbonate and nitrate in aqueous solutions: a study by ab initio quantum mechanical charge field molecular dynamics* J. Phys. Chem. B, **2011**, *115*, 12527–12536.
- [81] V. Vchirawongkwin, C. Kritayakornupong, V. Ruangpornvisuti, B. M. Rode *Inter- and intra-molecular OH stretching modes of bicarbonate in aqueous solution* J. Mol. Struct. (Theochem), **2009**, *913*, 236–239.

- [82] C. Kritayakornupong, V. Vchirawongkwin, T. S. Hofer, B. M. Rode *Structural and dynamical properties of hydrogen fluoride in aqueous solution: an ab initio quantum mechanical charge field molecular dynamics simulation* J. Phys. Chem. B, **2008**, *112*, 12032–12037.
- [83] C. Kritayakornupong, V. Vchirawongkwin, B. M. Rode *An ab initio quantum mechanical charge field molecular dynamics simulation of a dilute aqueous HCl solution* J. Comput. Chem., **2010**, *31*, 1785–1792.
- [84] V. Vchirawongkwin, A. B. Pribil, B. M. Rode *Ab initio quantum mechanical charge field study of hydrated bicarbonate ion: structural and dynamical properties* J. Comput. Chem., **2010**, *31*, 249–257.
- [85] A. Luzar, D. Chandler *Structure and hydrogen bond dynamics of water-dimethyl sulfoxide mixtures by computer simulations* J. Chem. Phys., **1993**, *98*, 8160–8173.
- [86] D. Xenides, B. R. Randolph, B. M. Rode *Structure and ultrafast dynamics of liquid water: a quantum mechanics/molecular mechanics molecular dynamics simulations study* J. Chem. Phys., **2005**, *122*, 174506.
- [87] A. J. Fischmann, L. Spiccia *The first homoleptic gold(I) thiosulfonate complex* Dalton Trans., **2011**, *40*, 4803–4805.

VITAE

Personal Details

Name	Ms.Montira Trinapakul
Date of birth	30 August 1988
Place of birth	Bangkok, Thailand
Address	1/20 Happyland Grand Ville village, soi. 53, Lat Phrao 101 road, Khlong Chan, Bangkapi, Bangkok 10240, Thailand
Telephone	089-780-8286
E-mail	montira_bell@hotmail, ts.montira@gmail.com

Education

2010-2014	M.Sc. in Chemistry at Chulalongkorn University, Bangkok, Thailand
2006-2010	B.Sc. (<i>2nd honours</i>) in Chemistry at Chulalongkorn University, Bangkok, Thailand
2000-2006	Triamudomsuksanomklao School, Bangkok, Thailand

Conference

Montira Trinapakul and Viwat Vchirawongkwin. *Structural and dynamical properties of hydrated thiosulfate anion in pre-equilibrium: ab initio quantum mechanical charge field molecular dynamic simulation*. Proceedings of Pure and Applied Chemistry International Conference 2013 (PACCON 2013), Chon Buri, Thailand, January 23-25, **2013**, pp 918-921.

Academic publication

Montira Trinapakul, Chinapong Kritayakornupong, Anan Tongraar and Viwat Vchirawongkwin. *Active site of the solvated thiosulfate ion characterized by hydration structures and dynamics*. Dalton Trans., **2013**, 42, 10807-10817.

Scholarship

- | | |
|--------------|--|
| 2006-present | Development and Promotion of Science and Technology (DPST) for Bachelor and Master of Science program at Chulalongkorn University, Thailand |
| 2013 | Japan Student Services Organization (JASSO) scholarship for short-termed study in the School of Materials Science at Japan Advanced Institute of Science and Technology (JAIST), Kanazawa City, Ishikawa Prefecture, Japan |